A THREE MILLION YEAR INTEGRATION OF THE EARTH'S ORBIT

THOMAS R. QUINN
Department of Astrophysics, Oxford University, Keble Road, Oxford OX1 3RH, England

SCOTT TREMAINE
Canadian Institute for Theoretical Astrophysics, McLennan Laboratories, University of Toronto, 60 St. George Street, Toronto, Ontario M5S 1A1, Canada

MARTIN DUNCAN
Department of Physics, Stirling Hall, Queen's University, Kingston, Ontario K7L 3N6, Canada
Received 16 November 1990; revised 11 February 1991

ABSTRACT

We have integrated the equations of motion of the nine planets and the Earth's spin axis for 3.05 million years into the past. The equations include the dominant relativistic corrections and corrections for the quadrupole moment of the Earth–Moon system; solar mass loss is neglected but the principal consequence of this neglect is an unimportant nonuniformity in the overall timescale of less than one part per million. The initial conditions are taken from the JPL DE 102 ephemeris. We believe that the heliocentric direction to the Earth and the direction of the Earth's pole are correct to within about 0.03 radians at the end of the integration; errors in the other planets are larger, because of larger integration errors (for Mercury) or less accurate initial conditions (for the outer planets). All the planetary orbits appear to be regular on this timescale (i.e., there is no evidence of exponential divergence in adjacent trajectories). We have computed the orbital elements of all the planets and the Earth's spin direction at 0.1 yr intervals and have removed short-term variations using a low-pass filter, in order to isolate the long-term variations (period >2000 yr). The smoothed elements are available at 500 yr intervals. They can be used to check or to replace the results of secular perturbation theory and as input to geophysical models that test the Milankovich hypothesis that climate variations are caused by changes in the Earth's orbit.

1. INTRODUCTION

Long integrations of the outer solar system (Jupiter to Pluto) have been carried out by Cohen *et al.* (1973; 1 Myr), Kinoshita & Nakai (1984; 5 Myr), Applegate *et al.* (1986; 217 Myr), the LONGSTOP collaboration (Roy *et al.* 1988; 100 Myr), and Sussman & Wisdom (1988; 845 Myr). Integrating the orbits of all nine planets is a more demanding task for several reasons: there are 45 mutual interactions between the planets and the Sun instead of 15; the shortest orbital period is almost a factor of 50 shorter (0.24 yr for Mercury compared to 11.86 yr for Jupiter); and the eccentricity of the innermost planet is larger (at present $e = 0.206$ for Mercury compared to 0.048 for Jupiter), which makes the orbit more difficult to integrate accurately.

The longest integration of all nine planets that is fit directly to observational data is the DE 102 ephemeris produced at JPL (Newhall *et al.* 1983), which covers the 4400 yr interval from 1411 BC to 3002 AD and includes both general relativistic corrections and an integration of the lunar orbit. Richardson & Walker (1987,1989) have integrated the orbits of the nine planets for a 2 Myr interval centered on the present, and Applegate *et al.* (1986) have integrated the orbits of all of the planets except Mercury for 3 Myr. These integrations are longer but less accurate than the DE 102 integration; they do not follow the lunar orbit and they neglect corrections like general relativity and the attraction of the Sun on the quadrupole moment of the Earth–Moon system, which affect the acceleration of the Earth by fractions $\simeq 10^{-8}$ and $\simeq 10^{-7}$, respectively.

There are several motivations for following the orbits of the planets over timescales of at least several Myr:

(i) According to the Milankovich hypothesis, climate variations on the Earth are caused by insolation changes arising from slow oscillations in the Earth's orbital elements and the direction of the Earth's spin (see Berger 1980 or Imbrie 1982 for a review). So far, the astronomical input to the geophysical models that are compared with the geological record (mainly the $^{18}O/^{16}O$ ratio in foraminifera shells obtained from seabed cores, which reflects the volume of water locked up in ice) is based on secular perturbation theory. It is important to check the accuracy of the perturbation theory and to provide the best possible orbital elements over the interval accessible to geological observation.

(ii) Pluto's orbit is chaotic, with an inverse Liapunov exponent (the *e*-folding time for divergence of nearby trajectories) of 20 Myr (Sussman & Wisdom 1988). Laskar (1989) has used secular perturbation theory to argue that the inner solar system is chaotic, with an inverse Liapunov exponent of only 5 Myr. Direct integrations can test Laskar's prediction (although the integrations described in this paper are not yet long enough to do so), and can search for chaotic motion with shorter *e*-folding times that may have been missed by his approximate theory.

(iii) Numerical integrations help guide the development of approximate analytic theories for the long-term behavior of the solar system.

This paper describes an accurate integration of the positions of the nine planets and the orientation of the Earth's pole over the past 3 Myr. "Accurate" can only be loosely defined in this context, but roughly speaking our design goal was that the errors in the Earth's longitude and pole position should be much less than 1 radian at the end of 3 Myr; in fact, we believe the error is $\lesssim 0.03$ radians. (Throughout this pa-

 0004-6256/91/062287-19$00.90

per, the term "Earth" often refers to the Earth–Moon barycenter, since we do not explicitly integrate the lunar orbit.) An obstacle to achieving this goal is solar mass loss, which can affect the longitude of the Earth by several radians over 3 Myr; however, we argue below that the principal effect of solar mass loss can be removed by introducing a slightly nonuniform timescale. Errors in the positions of the other planets are larger, due to less accurate numerical integration or initial conditions, but should still be $\lesssim 1$ radian for all planets except Mercury and Pluto, where the errors could be several radians.

The force per unit mass exerted on the Earth by the Sun is approximately $F_0 = G\mathcal{M}_\odot/a_\oplus^2$, where $a_\oplus$ is the Earth's semimajor axis. If we neglect an acceleration of magnitude ϵF_0, the resulting longitude error after time t should be about $2\pi\epsilon(t/1\text{ yr}) = (0.02\text{ rad})(\epsilon/10^{-9})(t/3\text{ Myr})$. Thus to achieve an error $\lesssim 0.03$ radians we must evaluate the total acceleration of the Earth to a fractional accuracy $\epsilon \lesssim 10^{-9}$.

2. EQUATIONS OF MOTION

2.1 Planetary Orbits

If we treat each planet as a point mass m_i with position $\mathbf{r}_i$ in a heliocentric frame, the Newtonian equations of motion read

$$\frac{d^2\mathbf{r}_i}{dt^2} = -\frac{G(\mathcal{M}_\odot + m_i)}{r_i^3}\mathbf{r}_i + \sum_{\substack{j=1\\ j\neq i}}^{9}\frac{Gm_j}{|\mathbf{r}_i - \mathbf{r}_j|^3}(\mathbf{r}_j - \mathbf{r}_i) - \sum_{\substack{j=1\\ j\neq i}}^{9}\frac{Gm_j}{r_j^3}\mathbf{r}_j. \quad (1)$$

The accuracy of our integration depends on the accuracy of the planetary masses m_i and the initial conditions $\mathbf{r}_i(t_0)$, $\dot{\mathbf{r}}_i(t_0)$. Both masses and initial conditions were taken from the DE 102 ephemeris. Although more accurate masses for the outer planets are now available (from the *Pioneer* and *Voyager* spacecraft and from observations of Pluto's satellite Charon), we preferred to use a consistently determined set of parameters. In any event the errors in the masses are at most $3\times10^{-7}\,\mathcal{M}_\odot$ (for Neptune and Pluto), so that the fractional error in the acceleration at the Earth due to mass errors is only about $\epsilon = 10^{-11}$ [the acceleration in a heliocentric frame at 1 A.U. due to a body at distance $r \gg 1$ A.U. is proportional to $(r/1\text{ A.U.})^{-3}$], which is well within our error budget $\epsilon \ll 10^{-9}$.

The initial conditions were taken from DE 102 at epoch $t_0 =$ JD 2433280.5 (near J1950.0 = JD 2433282.5), except that the position and velocity of the Earth–Moon barycenter are modified slightly to correct for our approximate treatment of the lunar orbit (see below). The formal standard deviations in the mean motions of the four inner planets (Standish 1990) lead to longitude errors <0.005 radians after 3 Myr. The uncertainties in the mean motions of the outer planets are larger, since their orbits are based on optical observations rather than spacecraft tracking or radar. The formal uncertainties given by Standish (1990) lead to longitude errors after 3 Myr of <0.015 radians (Jupiter, Saturn, Uranus), 0.2 radians (Neptune), and 1 radian (Pluto). Realistic errors are likely to be substantially larger than the formal uncertainties. Fortunately, the planets with the most uncertain orbits have relatively little influence on the inner solar system; in addition, the most important long-term perturbations are usually secular ones, which do not depend on the longitude of the planet.

Appendix B gives the initial positions and velocities of the planets and the Earth's initial spin direction in the DE 102 reference frame, which is close to 1950.0 equatorial coordinates. The Appendix also lists the final state, at JD $-$ 1113787075.5, 3.056 Myr earlier than the initial epoch.

The integration is carried out in distance and time units of one astronomical unit, A.U. $= 1.49597870\times10^{13}$ cm, and one day, $D = 86400$ s. In these units, $G\mathcal{M}_\odot = k^2$, where $k = 0.01720209895$ is the Gaussian gravitational constant. In cgs units, $G\mathcal{M}_\odot = k^2(\text{A.U.})^3D^{-2} = 1.32712438\times10^{26}$ cm^3 s^{-2}.

2.2 Small Effects on Planetary Orbits

Direct integration of the lunar orbit is computationally expensive, since the lunar orbital period is more than a factor of three shorter than any planet's. Therefore we have treated the effect of the Moon on the planetary orbits, which are minor in any case, using analytic approximations.

Since the Earth–Moon separation is small compared to interplanetary separations, we can approximate the effect of the Moon's mass $\mathcal{M}_L$ on the other planets to adequate accuracy by simply representing the Earth–Moon system as a point mass $\mathcal{M}_\oplus + \mathcal{M}_L$ at the Earth–Moon barycenter. However, the solar attraction on the Earth–Moon system must be treated more carefully; because of the finite size of the lunar orbit the solar attraction is slightly different from the attraction that would be felt by a point mass at the barycenter.

To make this correction we replace the Earth and Moon by rigid circular rings of masses $\mathcal{M}_\oplus$ and $\mathcal{M}_L$ and radii $R_\oplus$ and R_L, lying in the plane of the ecliptic and centered on the Earth–Moon barycenter. The approximation that the rings lie in the ecliptic is valid in a time-averaged sense because the precession rate of the lunar node on the ecliptic (period 18.7 yr) is much faster than the timescale for variations in the orientation of the ecliptic. In order that $R_\oplus$ and R_L represent the actual sizes of the orbits we must have $R_\oplus/R_L = \mathcal{M}_L/\mathcal{M}_\oplus$ and $R_\oplus + R_L = R$, where R is approximately the mean Earth–Moon separation. In this approximation the acceleration of the Earth–Moon system due to the Sun in a heliocentric frame can be written as

$$-\frac{G(\mathcal{M}_\odot + \mathcal{M}_\oplus + \mathcal{M}_L)}{r^3}\mathbf{r} - \frac{3G\mathcal{M}_\odot\mathcal{M}_\oplus\mathcal{M}_L}{4(\mathcal{M}_\oplus + \mathcal{M}_L)^2}\frac{R^2}{r^5}f\mathbf{r}, \quad (2)$$

where $r = |\mathbf{r}|$, $\mathbf{r}$ is the vector from the Sun to the Earth–Moon barycenter, and $f \simeq 1$ is a correction factor that we discuss below. We have neglected contributions of higher order in R/r, whose effects are smaller by $O(R/r)^2 \simeq 10^{-5}$, as well as corrections of higher order in $(\mathcal{M}_\oplus + \mathcal{M}_L)/\mathcal{M}_\odot$ arising from the transformation from inertial to heliocentric frames. The first (monopole) term is the acceleration that would be felt by a point mass at the barycenter, and the second (quadrupole) term describes an extra acceleration of fractional size $\epsilon \simeq 6\times10^{-8}$.

The correction factor f arises because the average lunar orbit cannot be represented exactly as a circular ring in the ecliptic. Its value depends on our choice for R since only the combination R^2f enters Eq. (2). We adopt $R(t_0) \equiv R_0 = 3.8440\times10^{10}$ cm $= 0.0025696$ A.U. at the in-

itial epoch t_0 and $f = 0.9473$; the Earth–Moon mass ratio is taken to be $\mathcal{M}_\oplus/\mathcal{M}_L = 81.3007$ as in DE 102 (see Appendix A for details).

The radius R increases as the lunar orbit recedes due to tidal friction. At present, the lunar mean motion is decreasing at a rate

$$(\dot{n}_L/n_L)_0 = -(4.6 \pm 0.2)\times 10^{-18}\ \mathrm{s}^{-1} \tag{3}$$

(Dickey & Williams 1982). Using the Kepler relation $\dot{R}/R = -\frac{2}{3}(\dot{n}_L/n_L)$, we may represent the change in the Earth–Moon distance as

$$R(t) = R_0\left[1 - \tfrac{2}{3}(\dot{n}_L/n_L)_0 (t - t_0)\right], \tag{4}$$

where we have approximated $R(t)$ as a linear function of time. Over 3 Myr, the fractional change in R is 3×10^{-4}, which has a negligible effect on the acceleration of the Earth–Moon system but does affect the precession of the spin axis (Sec. 2.3).

A final correction to the orbit of the Earth–Moon barycenter arises because the semimajor axis of the barycenter oscillates with an amplitude of about 10^{-8} A.U. and a period of one synodic month. By approximating the Moon as a ring, we have removed this oscillation, and we must adjust the initial conditions to remove the oscillation as well. We do so by replacing the initial position $\mathbf{r}$ and velocity $\mathbf{v}$ by $(1+\delta)\mathbf{r}$ and $(1-\frac{1}{2}\delta)\mathbf{v}$ where $\delta = -4.83\times 10^{-9}$ (see Appendix A).

Corrections due to general relativity yield fractional accelerations of order $\epsilon = G\mathcal{M}_\odot/(c^2 a_\oplus) \simeq 10^{-8}$. Only relativistic corrections due to the Sun are important; corrections due to the other planets are down by a further factor of 10^3 or more and can safely be ignored. The additional acceleration is given by (Newhall *et al.* 1983; Will 1981)

$$\frac{d^2\mathbf{r}_i}{dt^2} = \frac{G\mathcal{M}_\odot}{r_i^3}\mathbf{r}_i\left(2(\beta_{\mathrm{ppn}}+\gamma_{\mathrm{ppn}})\frac{G\mathcal{M}_\odot}{c^2 r_i} - \gamma_{\mathrm{ppn}}\frac{v_i^2}{c^2}\right) + (2+2\gamma_{\mathrm{ppn}})\frac{G\mathcal{M}_\odot}{c^2 r_i^3}\mathbf{v}_i(\mathbf{r}_i\cdot\mathbf{v}_i). \tag{5}$$

Here β_{ppn} and γ_{ppn} are PPN parameters; they equal unity in general relativity, which we assume to be correct. The speed of light is $c = 2.99792458\times 10^{10}$ cm s^{-1}.

The mass of the largest asteroid, Ceres, is $m = (5.0 \pm 0.2)\times 10^{-10}\mathcal{M}_\odot$ (Standish & Hellings 1989), and it contributes only a fraction $\epsilon \simeq (m/\mathcal{M}_\odot)(1\ \mathrm{A.U.}/a)^3 = 2\times 10^{-11}$ to the acceleration of the Earth. The total mass of the asteroid belt is not well known but its contribution to the Earth's acceleration is negligible in the likely case that its total mass is no more than a few times the mass of Ceres.

Accelerations due to comets, passing stars, and the overall tidal field of the Galaxy are negligible.

The Sun loses mass at a rate $\dot{\mathcal{M}}/\mathcal{M}_\odot = 7\times 10^{-14}$ yr$^{-1} \equiv \tau^{-1}$, mostly due to electromagnetic radiation. In the absence of mutual planetary perturbations, slow mass loss leads to expansion of the planetary orbits ($a \propto \mathcal{M}^{-1}$) at constant eccentricity. The orbital periods P increase in proportion to $\mathcal{M}^{-2}$, leading to a longitude difference after time t of $\Delta\phi = -2\pi t^2/(P\tau) = -4.0(t/3\ \mathrm{Myr})^2(1\ \mathrm{yr}/P)$ radians. Thus, in a strict sense, the solar mass-loss rate is sufficiently high that the longitudes of the inner planets are inaccurate within a few Myr. On the other hand, the longitude traveled in a time interval Δt is $\Delta\phi = 2\pi\Delta t/P$, so the change in the configuration of the planets caused by solar mass loss is nearly the same as the change caused by a clock error $\Delta t = -t^2/\tau$. Thus, to first order, an integration that neglects solar mass loss will produce the correct relative configurations of the planets but at a slightly incorrect time, and the correction is simple to compute if τ is known. Other errors with different scalings arise because of mutual planetary perturbations, but these errors are insignificant over a few Myr interval. For example, the secular precession periods vary as $\mathcal{M}^{-1}$, not $\mathcal{M}^{-2}$, leading to an error in the periapse $\Delta\varpi = -\pi t^2/(P_s\tau)$ where P_s is the precession period; for the shortest precession period, $P_s \simeq 5\times 10^4$ yr, $\Delta\varpi = 4\times 10^{-5}$ radians after 3 Myr, which is negligible. With these arguments as justification, we shall neglect solar mass loss.

Including the effects discussed above, the equations of motion become

$$\frac{d^2\mathbf{r}_i}{dt^2} = -\frac{G(\mathcal{M}_\odot + m_i)}{r_i^3}\mathbf{r}_i + \sum_{\substack{j=1\\ j\neq i}}^{9}\frac{Gm_j}{|\mathbf{r}_i - \mathbf{r}_j|^3}(\mathbf{r}_j - \mathbf{r}_i) - \sum_{\substack{j=1\\ j\neq i}}^{9}\frac{Gm_j}{r_j^3}\mathbf{r}_j + \frac{G\mathcal{M}_\odot}{r_i^3}\mathbf{r}_i\left(2(\beta_{\mathrm{ppn}}+\gamma_{\mathrm{ppn}})\frac{G\mathcal{M}_\odot}{c^2 r_i} - \gamma_{\mathrm{ppn}}\frac{v_i^2}{c^2}\right) + (2+2\gamma_{\mathrm{ppn}})\frac{G\mathcal{M}_\odot}{c^2 r_i^3}\mathbf{v}_i(\mathbf{r}_i\cdot\mathbf{v}_i) - \frac{3}{4}\delta_{i3}\frac{G\mathcal{M}_\odot}{r_i^3}\mathbf{r}_i\left(\frac{R}{r_i}\right)^2 f\frac{\mathcal{M}_\oplus\mathcal{M}_L}{(\mathcal{M}_L+\mathcal{M}_\oplus)^2}. \tag{6}$$

2.3 The Earth's Spin Axis

The precession of the Earth's spin axis is mostly determined by torques from the Moon and Sun, with a small contribution from general relativity.

We treat the lunar torques by once again replacing the Moon by a ring, surrounding and centered on the Earth. The lunar node precesses around the ecliptic in 18.7 yr; in principle we could follow the nodal precession but there is no substantial loss of accuracy if instead we use a ring lying in the plane of the Earth's orbit and assume that the ring remains in this plane as the orbit changes.

Let $\hat{\mathbf{a}}$, $\hat{\mathbf{b}}$ be normals to the Earth's equator and the instantaneous ecliptic (i.e., the unit vector $\hat{\mathbf{b}}$ is parallel to $\mathbf{r}\times\mathbf{v}$, where $\mathbf{r}$ and $\mathbf{v}$ are the heliocentric position and velocity of the Earth–Moon barycenter). Then

$$\frac{d\hat{\mathbf{a}}}{dt} = K(t)\left[2(1\ \mathrm{A.U.}/r)^3(\hat{\mathbf{r}}\cdot\hat{\mathbf{a}})(\hat{\mathbf{r}}\times\hat{\mathbf{a}}) - \beta_L(t)\times(\hat{\mathbf{b}}\cdot\hat{\mathbf{a}})(\hat{\mathbf{b}}\times\hat{\mathbf{a}})\right] + \frac{3G\mathcal{M}_\odot}{2r^3c^2}(\mathbf{r}\times\mathbf{v})\times\hat{\mathbf{a}}, \tag{7}$$

where the three terms describe, respectively, torques due to the Sun and Moon (e.g., Goldreich 1966) and the geodetic

precession (e.g., Weinberg 1972). The parameters K and β_L are time dependent because the lunar orbit recedes from the Earth due to tidal friction.

The factor $K(t)$ at the present time is given by

$$K(t_0) \equiv K_0 = \frac{3}{2} \frac{G\mathcal{M}_\odot}{\omega(1\ \text{A.U.})^3} \frac{C-A}{C}, \tag{8}$$

where $(C-A)/C = 0.0032739935$ is the dynamical ellipticity of the Earth and $\omega = 7.29211515 \times 10^{-5}\ \text{s}^{-1}$ is the mean spin of the Earth (e.g., Kubo & Fukushima 1988). Thus $K_0 = 2.669629 \times 10^{-12}\,\text{s}^{-1}$. The factor β_L is more difficult to evaluate because of the complexities of the lunar orbit. It may be written in the form

$$\beta_L(t_0) \equiv \beta_{L,0} = g \frac{\mathcal{M}_L}{\mathcal{M}_\odot} \left(\frac{1\ \text{A.U.}}{R_0} \right)^3, \tag{9}$$

where R_0 is a measure of the radius of the lunar orbit (see Sec. *2.2* and Appendix A) and $g = 0.9925194$ according to Kinoshita (1975, 1977).[1] Evaluating Eq. (9) yields $\beta_{L,0} = 2.161225$.

As a check we can compute the rate of luni-solar precession,

$$\psi = K(\kappa + \beta_{L,0}) \cos\epsilon + \gamma_{\text{gp}}, \tag{10}$$

where $\kappa = (1\ \text{A.U.}/a)^3(1-e^2)^{-3/2}$, a and e are the semi-major axis and eccentricity of the Earth's orbit, $\epsilon = \cos^{-1}(\hat{\mathbf{a}}\cdot\hat{\mathbf{b}})$ is the Earth's obliquity, and γ_{gp} is the correction for geodetic precession. From Eq. (7), it is easy to show that $\gamma_{\text{gp}} = -\frac{3}{2}(G\mathcal{M}_\odot)^{3/2} a^{-5/2}/c^2$, in the approximation where the Earth's mass and orbital eccentricity are neglected. At the epoch J2000.0, we have $\kappa = 1.000419$, $\epsilon = 23.43929°$, $\gamma_{\text{gp}} = 1.92$ arcsec per Julian century, and we find $\psi = 5038.78$ arcsec per Julian century, which is the usual value for the luni-solar precession (Lieske *et al.* 1977). (Of course, the agreement is expected, since the dynamical ellipticity is computed from the observed precession.) This is an important check, for the following reason: if the Earth's orbit and the lunar orbit are approximated as fixed, then errors in the *relative* contribution of solar and lunar torques, or the neglect of torques from other sources, are unimportant so long as the *total* torque—which is precisely what is measured by the rate of luni-solar precession—is correct.

The recession of the lunar orbit due to tidal friction causes slow changes in $K(t)$ and $\beta_L(t)$. The dynamical ellipticity $(C-A)/C$ is proportional to ω^2 and hence from Eq. (8) we have $\dot{K}/K = \dot{\omega}/\omega$. Similarly $\dot{\beta}_L/\beta_L = -3\dot{R}/R = 2\dot{n}_L/n_L$, where n_L is the lunar mean motion. The changes are slow enough that we can represent K and β_L as linear functions of time,

$$\begin{aligned} K(t) &= K_0[1 + (\dot{\omega}/\omega)_0 (t - t_0)], \\ \beta_L(t) &= \beta_{L,0}[1 + 2(\dot{n}_L/n_L)_0 (t - t_0)]. \end{aligned} \tag{11}$$

We take $(\dot{n}_L/n_L)_0$ from Eq. (3) and $(\dot{\omega})_0 = 51(\dot{n}_L)_0$ (Lambeck 1980). Finally, tides decrease the obliquity at a rate given by

$$\frac{d\hat{\mathbf{a}}}{dt} = -\hat{\mathbf{c}} \frac{d\epsilon}{dt}, \tag{12}$$

where $\hat{\mathbf{c}} = [\hat{\mathbf{b}} - (\hat{\mathbf{a}}\cdot\hat{\mathbf{b}})\hat{\mathbf{a}}]/\sin\epsilon$ and $\dot{\epsilon} = -4.17 \times 10^{-19}\ \text{s}^{-1}$ (Lambeck 1980).

So far we have not distinguished the mean spin axis of the Earth from the instantaneous spin axis. The difference is due to nutation, the short-period oscillations due to torques from the Sun and Moon. The largest nutational component has an amplitude of 9.2 arcsec. The spin axis $\hat{\mathbf{a}}$ that we are following is neither the instantaneous axis nor the mean axis. By replacing the Moon by a ring lying in the ecliptic, we have eliminated all terms in the nutation that involve the lunar longitude, pericenter, or node, but we have not eliminated terms depending only on the solar longitude or solar mean anomaly. The largest remaining component has an amplitude of 0.55 arcsec and a period of six months. The initial spin given in Appendix B is obtained from the initial mean spin in DE 102, $\hat{\mathbf{a}} = (0,0,1)$ at B1950.0, by precessing the mean spin to our initial epoch using the formulas in Sec. *3.6*, then correcting for the 0.55 arcsec component of the nutation.

3. NUMERICAL TECHNIQUES AND ACCURACY TESTS

3.1 Integration Method

The integrations of the planetary orbits were carried out using explicit multistep methods of the form

$$x_{n+1} = -\sum_{j=1}^{k} \alpha_{k-j} x_{n-j+1} + h^2 \sum_{j=1}^{k} \beta_{k-j} f_{n-j+1}, \tag{13}$$

where x_n is one of the Cartesian components of the planet's position at step n, $h = t_{n+1} - t_n$ is the fixed stepsize, and f_n is the corresponding component of the acceleration at step n. We have used two methods:

(i) Störmer method with $k = 13$. This method has $\alpha_{k-1} = -2$, $\alpha_{k-2} = 1$, and $\alpha_{k-3} = \cdots = \alpha_0 = 0$. The Störmer method has been used successfully in many solar system integrations (Cohen *et al.* 1973; Kinoshita & Nakai 1984; Applegate *et al.* 1986; Sussman & Wisdom 1988). The coefficients are chosen so that the method integrates a 14th-order polynomial exactly, and are given by Cohen *et al.* (1973).

(ii) Symmetric method with $k = 12$. Symmetric methods have $\alpha_j = \alpha_{k-j}$, $\beta_j = \beta_{k-j}$, $\alpha_0 = 1$, $\beta_0 = 0$ (Lambert & Watson 1976); the coefficients are chosen so that the method integrates a 13th-order polynomial exactly (Quinlan & Tremaine 1990).

The 3 Myr integration was carried out with the symmetric method and a step size $h = 0.75$ days. Shorter integrations using the Störmer method were carried out as accuracy checks (see below). Over the longest interval tested, the accuracy of the symmetric method with stepsize h appeared to be about the same as the accuracy of the Störmer method with stepsize $0.6h$.

We have also experimented with the use of implicit methods for the orbit integrations, by adding a corrector step after each predictor step (13). This requires at least two force evaluations per timestep and we have found that the computing resources required for the extra force evaluation are better spent on an explicit method with a smaller timestep.

The velocity is evaluated at each timestep to compute the PPN corrections (5), using the formula

$$v_{n+1} = h^{-1}\left(x_n - x_{n-1} + h^2 \sum_{j=1}^{13} \gamma_{k-j} f_{n-j+1} \right); \tag{14}$$

[1] The factor g is twice the factor in square brackets in Eq. (10.1) of Kinoshita 1977. We have used constants $M_0 - \frac{1}{2}M_2 = 0.4963034$, $M_1 = -2.07 \times 10^{-5}$, and $M_3 = 2.992 \times 10^{-3}$ from Kinoshita (1975).

the coefficients γ are given by Cohen *et al.* (1973).

The evolution of the Earth's spin axis $\hat{\mathbf{a}}$ [Eq. (7)] was followed using an Adams–Bashforth predictor of the form

$$a_{n+1} = a_n + h \sum_{j=1}^{13} \delta_{k-j} f_{n-j+1}, \tag{15}$$

where a is one Cartesian component of $\hat{\mathbf{a}}$ and f_n is the rate of change of that component at step n. In this case we found that a corrector step was needed for stability; thus, after the update of the planetary positions and spin to timestep $n+1$, the rate of change of the spin axis at timestep $n+1$ was calculated, and a single Adams–Moulton corrector step was applied to the spin axis, using the equation

$$a_{n+1} = a_n + h \sum_{j=1}^{13} \zeta_{k-j} f_{n-j+2}. \tag{16}$$

Prescriptions for computing the coefficients δ and ζ in Eqs. (15) and (16) are given by Gear (1971).

The multistep integrator was started using the procedure given by Cohen *et al.* (1973): we integrated the positions 12 steps forward using the Cowell corrector formula, assuming that the acceleration was equal to its initial value. New accelerations were then calculated and extrapolated backwards using a polynomial of degree 12. A new integration was then carried out from the initial time forward to step 12, and the process was iterated to convergence. A similar procedure was used to start the spin axis integration.

3.2 Roundoff Error

We first state some general results about roundoff error in floating-point arithmetic. Floating-point numbers are stored in the computer in the form $\pm \Sigma_{i=0}^{p-1} a_i 2^{e-i}$, where $a_0 = 1$, $a_i = 0$ or 1 for $i > 0$, and e is an integer. Real numbers of this form are called representable numbers; real numbers that are not representable are rounded by the machine to one of the two adjacent representable numbers. We denote the rounded value of x by $rnd(x)$. If A is any arithmetic expression involving representable numbers and arithmetic operators, then $fl(A)$ is the representable number that is obtained by evaluating this expression on the computer. Floating-point arithmetic is said to be optimal if for all expressions A, $fl(A)$ is the representable number nearest to the exact value of A.

Dekker (1971; see also Knuth 1981 and Quinn & Tremaine 1990) has shown that if u and v are representable, $|u| \geqslant |v|$, and floating-point arithmetic is optimal, then the roundoff error in adding u and v is

$$(u+v) - fl(u+v) = fl\{v - fl\,[\,fl(u+v) - u\,]\}. \tag{17}$$

Thus it is possible to define a function

$$err_+(x_1,\ldots,x_n) = (x_1 + \cdots + x_n) - fl(x_1 + \cdots + x_n) \tag{18}$$

that evaluates the roundoff error in a summation using ordinary floating-point arithmetic.

Roundoff can be the dominant source of error in long solar system integrations, and hence we have attempted to minimize roundoff error in our calculations. All of our integrations were carried out on machines compliant with the ANSI/IEEE (1985) Standard 754 for floating-point arithmetic. Among other features, this standard requires that (i) floating-point arithmetic is optimal; (ii) rounding is done by the "round-to-even" algorithm, that is, $rnd(x)$ is the representable number closest to x, and if the two adjacent representable numbers are equidistant, then the one with its least significant bit equal to zero is chosen. The round-to-even algorithm minimizes systematic bias in additions.

Several additional steps were taken to control roundoff error in evaluating equation (13):

(i) The coefficients α_{k-j} were restricted to powers of 2 so that the multiplications $\alpha_{k-j} x_{n-j+1}$ are done exactly in binary arithmetic (this condition is automatically satisfied by the Störmer method but restricts the choice of symmetric method; see Quinlan & Tremaine 1990).

(ii) The roundoff error arising in the additions in the first summation in Eq. (13) was monitored using the function err_+. The part of the error that exceeded one significant bit was added back into the sum and the residual error was propagated ahead to the next timestep (see Quinn & Tremaine 1990 for details). The roundoff arising in the addition of the first sum in (13) to the second sum was corrected in the same way. Cohen *et al.* (1973) and Applegate *et al.* (1986) also suppressed roundoff errors in these sums, the latter using the function err_+.

[iii(a)] A source of systematic roundoff bias is the imprecise representation of the coefficients β_{k-j}. This error can be eliminated by evaluating the difference $\delta\beta_{k-j} = \beta_{k-j} - rnd(\beta_{k-j})$. The summation $\Sigma \delta\beta_{k-j} f_{n-j+1}$ then yields the total roundoff error arising from this source. The part of this error that exceeded one significant bit was added back to Eq. (13) and the residual error was propagated ahead to the next timestep (Quinn & Tremaine 1990).

[iii(b)] A faster but less accurate way to eliminate bias arising from imprecise representation of the coefficients β_{k-j} is to exploit the fact that they are rational numbers with a common denominator, $\beta_{k-j} \equiv n_{k-j}/m$. Thus the second sum in Eq. (13) may be written $(h^2/m)\Sigma_{j=1}^{k} n_{k-j} f_{n-j+1}$. The integers n_{k-j} are represented exactly and hence there is no systematic bias in evaluating the sum; the bias arising from evaluating the quotient h^2/m only affects the overall timescale slightly and hence is unimportant. This technique was also used by Applegate *et al.* (1986).

(iv) Roundoff also arises in the additions in the second summation in Eq. (13). Although this sum is multiplied by the small number h^2, the error that arises in this way is enhanced by partial cancellations, which arise because the coefficients β_{k-j} are large and alternating in sign: thus $\max |\beta_{k-j}| / \Sigma_{j=1}^{k} \beta_{k-j} = 101.9$ for the $k = 13$ Störmer method (the analogous ratio for the $k = 12$ symmetric method is only 6.35, so the symmetric method is less sensitive to cancellation). This error can be corrected using the method described in (ii).

All of these errors arise in the integration algorithm. Roundoff errors also arise in the evaluation of the accelerations; these are more difficult to remove but fortunately appear to be less serious than the correctable errors that we have described.

Some of our integrations employ corrections (i)–(iv), following the prescription in Quinn & Tremaine (1990). However, later experiments by Quinlan (1990) show that the use of [iii(b)] instead of [iii(a)] and the elimination of (iv) still gave satisfactory results with the symmetric method, and this is the procedure used in the runs described below that are based on the symmetric method.

No roundoff corrections were used during the startup procedure, nor were roundoff corrections used in evaluating the

velocities that are used to compute the relativistic corrections in Eq. (5).

3.3 The 3 Myr Integration

Our longest integration was carried out using the symmetric method with stepsize $h = 0.75$ days. The integration was started at t_0 = JD 2433280.5; the integrations first went forward in time to t_b = JD 5812924.5 (an interval of 9252.96 Julian years), and then back in time to t_f = JD $-$ 1113787075.5, an interval of 3.056×10^6 Julian years. The initial integration to t_b ensured that the filter array used to produce smoothed orbital elements (Sec. *3.4*) was filled before the main integration reached t_0, so that smoothed elements would be available beginning at t_0. The initial conditions and final state are given in Appendix B.

The phase space coordinates of all the planets and the direction of the Earth's spin axis were output at intervals of 720 000 days (1971.25 yr). The smoothed orbital elements described in Sec. *3.4* were output at intervals of 180 000 days (492.8 yr).

The integration was stopped seven times due to power failures, rebooting, or deliberate restarts (for reasons given below), at times (measured backwards from the start of the integration) of 0.527, 0.710, 1.018, 1.459, 1.887, 2.227, and 2.676 Myr. Each time the integration was restarted using the startup procedure described in Sec. *3.1*. The starting point was chosen roughly 10^4 yr from the last point of the previous integration, so that the time needed to refill the filter array did not lead to a gap in the smoothed output.

The 3 Myr integration was carried out mostly on a Silicon Graphics 4D-25 workstation. The workstation was also used for interactive work but for no other long background jobs. The integration was completed in roughly 65 days of machine time.

3.4 Long-Term Variations of Orbital Elements

Variations in the orbital elements of the planets occur on two distinct timescales: "fast" variations are associated with terms in the disturbing function involving the planetary longitudes, and generally have periods comparable to the orbital periods; while "slow" variations are associated with terms involving only the orientations of the nodes and apses, and have periods exceeding 10^4 yr. Variations in the direction of the Earth's spin axis have periods similar to those of the slow variations.

To study the long-term behavior of the solar system it is useful to isolate the slow variations, by applying a low-pass filter that smooths the elements by suppressing the spectral features associated with the fast variations.

Let $w(t)$ be any orbital element (the ones we use are the semimajor axis a, $k_{\rm eq} = e\cos\varpi_{\rm eq}$, $h_{\rm eq} = e\sin\varpi_{\rm eq}$, $p_{\rm eq} = \sin(\frac{1}{2}I_{\rm eq})\sin(\Omega_{\rm eq})$, $q_{\rm eq} = \sin(\frac{1}{2}I_{\rm eq})\cos(\Omega_{\rm eq})$, where e is the eccentricity, $I_{\rm eq}$ is the inclination, $\varpi_{\rm eq} = \omega_{\rm eq} + \Omega_{\rm eq}$, $\omega_{\rm eq}$ is the argument of perihelion, and $\Omega_{\rm eq}$ is the longitude of the ascending node, all measured in the DE 102 coordinate system, which is close to 1950.0 equatorial coordinates. We evaluate the orbital elements from the phase space coordinates at evenly spaced time intervals,

$$w_k \equiv w(t_0 + k\Delta t), \quad k = 0,...,N-1, \tag{19}$$

where N is the number of data points. The continuous Fourier transform (FT) of $w(t)$ is

$$W(f) = \int_{-\infty}^{\infty} w(t)e^{2\pi ift}dt,$$
$$w(t) = \int_{-\infty}^{\infty} W(f)e^{-2\pi ift}df. \tag{20}$$

The discrete FT of w_k is

$$W_n = \sum_{k=0}^{N-1} w_k e^{2\pi ikn/N},$$
$$w_k = \frac{1}{N}\sum_{n=0}^{N-1} W_n e^{-2\pi ikn/N}. \tag{21}$$

Note that $W_{n+N} = W_n$ so that we can restrict our attention to the interval $n = 0,...,N-1$ (see, for example, Press *et al.* 1986 for a general discussion of Fourier transforms).

For large N, the discrete FT W_n contains a component proportional to the continuous FT $W(f)$ evaluated at the frequency $f = f_s n/N$, where the sampling frequency is

$$f_s = 1/\Delta t; \tag{22}$$

however, the discrete FT also contains contributions from all other frequencies differing from $f_s n/N$ by an integer multiple of the sampling frequency ("aliasing"). Since $W(-f) = W^*(f)$ when $w(t)$ is real, there are also contributions from $W(-f)$ and its aliases as well. Thus, the sampling frequency f_s should be chosen so that no fast variations are aliased into the frequency range of the slow variations. In particular, we shall attempt to minimize aliasing into the frequency interval $|f| \leqslant f_l \equiv 1/2000$ yr (we shall call this the "slow" band); f_l is conservatively chosen to be more than a factor of 10 larger than the highest secular precession frequency. We have chosen $f_s = 1/(36\text{ days}) = 10.14\text{ yr}^{-1}$, which is small enough that the computation of the orbital elements—once every 48 steps for $h = 0.75$ days—does not slow the integration substantially, but large enough that there is very little chance that any spectral feature with substantial power will be aliased into the slow band ($f_l/f_s = 5\times10^{-5}$). As a direct check we have confirmed that there is no aliasing into the slow band for frequencies of the form $m/P_i - (m+k)P_j$, where the P's are orbital frequencies of the nine planets, and $|m| \leqslant 10$, $|k| \leqslant 3$.

It is cumbersome to store the output of the entire 3 Myr integration with this sampling frequency (required storage $\approx 10^{10}$ bytes). Instead we apply a linear nonrecursive filter in the time domain to remove high frequencies, then keep only one step out of every K ("decimation"), and repeat the filtering and decimation process until the sampling interval is long enough that the storage requirements are modest (this approach follows Carpino *et al.* 1987). Thus the goal of the filtering/decimation process is to (i) reduce the sampling interval to about 500 yr (which implies storage requirements of a few times 10^6 bytes only); (ii) suppress the fast variations (say, those with periods shorter than a few hundred years); (iii) avoid aliasing any spectral features into the slow band; (iv) avoid distorting any variations within the slow band.

We filter the output by replacing the data points w_k by

$$\tilde{w}_k = \sum_{m=-M}^{M} d_m w_{k-m}. \tag{23}$$

When $N \gg M$ we have to a good approximation

$$\tilde{W}_n = D_n W_n, \tag{24}$$

where $\tilde{W}_n$ and D_n, are the discrete FTs of $\tilde{w}_m$ and d_m. We must choose $\{d_m\}$ so that D_n is a suitable low-pass filter. The performance of the filter is specified by the ripple r in the passband x_p and the suppression s in the stop band $x_{\rm stop}$, that is, we require

$$|D(f) - 1| \leqslant r, \quad \text{for } |f/f_s| < x_p;$$
$$|D(f)| \leqslant s, \quad \text{for } x_{\rm stop} < |f/f_s| < 1 - x_{\rm stop}; \tag{25}$$

where in the discrete FT $f/f_s = n/N$.

We base our filters on the Kaiser window (e.g., Hamming 1983),

$$d_m = C \frac{\sin 2\pi m x_0}{\pi m} I_0(\beta\sqrt{1 - m^2/M^2}), \tag{26}$$

where I_0 is a modified Bessel function and C is a normalizing constant chosen so that $\Sigma_{m=-M}^{M} d_m = 1$. The filter has three free parameters, β, x_0, and M. The parameters $M = 80$, $x_0 = 0.024$, $\beta = 10$ (filter A) yield a ripple and suppression $r_A = 3.5\times10^{-5}$, $s_A = 1\times10^{-5}$ for passband and stop band $x_{p,A} = 0.005$ and $x_{{\rm stop},A} = 0.05$. Similarly, the parameters $M = 80$, $x_0 = 0.10$, $\beta = 20$ (filter B) yield $r_B < 10^{-9}$, $s_B < 10^{-9}$ for $x_{p,B} = 0.05$ and $x_{{\rm stop},B} = 0.15$. The Fourier transforms $D(f)$ for these filters are shown in Fig. 1.

First apply filter A to the output data. The slow frequency band is given in units of the original sampling frequency $f_{s,0} = 1/36$ days $= 10.14$ yr^{-1} by $f_l/f_{s,0} = 5\times10^{-5}$, which lies well within the passband $x_{p,A} = 0.005$ of filter A, so frequencies in this band are distorted by $\leqslant r_A = 3.5\times10^{-5}$. Filter A suppresses all frequencies $|f| > f_{{\rm max},0} \equiv f_{s,0} x_{{\rm stop},A} = 0.51$ yr^{-1} by a factor of at least s_A, so it is unlikely that any substantial power is left at periods shorter than 2 yr.

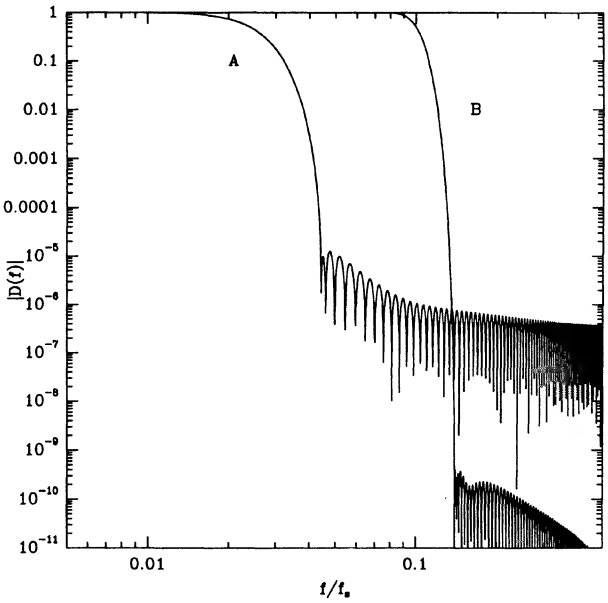

FIG. 1. The absolute values of the Fourier transforms of the filters A and B based on Eq. (26). The parameters of the filters are: $M = 80$, $x_0 = 0.024$, $\beta = 10$ (filter A); and $M = 80$, $x_0 = 0.10$, $\beta = 20$ (filter B). The frequency f is given in units of the sampling frequency $f_s = 1/\Delta t$. In the filter A passband ($f/f_s < 0.005$), $|D_A(f)|$ differs from unity by $< 3.5\times10^{-5}$; in the filter B passband ($f/f_s < 0.05$), $|D_B(f)$ differs from unity by $< 10^{-9}$

Now decimate by retaining only one out of every $K = 10$ steps. The new sampling interval is $\Delta t_1 = 10\Delta t = 1.0$ yr. The decimation creates new aliased frequencies. The effects of aliasing are easy to evaluate because the spectrum now has negligible power at frequencies $> f_{{\rm max},0} = 0.51$ yr^{-1}; the condition that there is no aliasing into the slow band is (e.g., Carpino *et al.* 1987)

$$f_s > f_l + f_{\rm max}, \tag{27}$$

which is easily satisfied for the new sampling frequency $f_{s,1} = 1/\Delta t_1 = 1.0$ yr^{-1}.

Next we repeat the process, applying filter A once again to the decimated data. The slow frequency band in units of the sampling frequency is now $f_l/f_{s,1} = 5\times10^{-4}$, which still lies well within the passband $x_{p,A} = 0.005$. The filter suppresses frequencies $|f| > f_{{\rm max},1} \equiv f_{s,1} x_{{\rm stop},A} = 0.051$ yr^{-1}, corresponding to periods shorter than about 20 yr.

Now decimate once again with $K = 10$, so that the new sampling interval is $\Delta t_2 = 10\Delta t_1 = 10$ yr. This again creates new aliased frequencies but none in the slow band as shown by Eq. (27) with $f_{s,2} = 0.10$ yr^{-1}, $f_{{\rm max},1} = 0.051$ yr^{-1}.

Now filter and decimate a third time with filter A and $K = 10$. The slow band still lies within the passband since $f_l/f_{s,2} = 0.005 = x_{p,A}$. The filter suppresses all frequencies $|f| > f_{{\rm max},2} \equiv f_{s,2} x_{{\rm stop},A} = 0.0051$ yr^{-1}. Decimation makes the sampling interval $\Delta t_3 = 10\Delta t_2 \simeq 100$ yr. The new aliased frequencies do not lie in the slow band, as shown by Eq. (27) with $f_{s,3} = 0.01$ yr^{-1}, $f_{{\rm max},2} = 0.0051$ yr^{-1}.

We filter a final time using filter B. The slow band is still in the passband since $f_l/f_{s,3} = 0.05 = x_{p,B}$. The filter suppresses all frequencies $|f| > f_{{\rm max},3} \equiv f_{s,3} x_{{\rm stop},B} = 0.0015$ yr^{-1}. Now decimate using $K = 5$, so that $\Delta t_4 = 5\Delta t_2 \simeq 500$ yr. The new aliased frequencies do not lie in the slow band, as shown by (27) with $f_{s,4} = 0.002$ yr^{-1}, $f_{{\rm max},3} = 0.0015$ yr^{-1}.

Thus we have accomplished the goals of the filtering/decimation process: (i) our sampling interval is now $\Delta t_4 = 492.8$ yr, long enough so that storage requirements for the output are modest; (ii) all variations with period shorter than $1/f_{{\rm max},3} = 657$ yr are suppressed by at least a factor $s_B < 10^{-9}$; (iii) no fast variations have been aliased into the slow band $|f| \leqslant f_l = 1/(2000\,{\rm yr})$; and (iv) the fractional distortion of the signal within the slow band is less than $3r_A + r_B = 1\times10^{-4}$.

In order for filtered elements to be available starting at the initial epoch, we must first integrate forwards in time for an interval $93879\Delta t$ before beginning to integrate backwards in time.

As a check on this procedure, we have generated an artificial signal which is the sum of six sinusoids of unit amplitude; three of the sinusoids have periods within the slow band (periods 1.3×10^5 yr, 3.3×10^4 yr, and 2.1×10^3 yr), and three have shorter periods (500, 36, and 0.9 yr). The signal is passed through the filter/decimation process described above, and the output signal is compared to the sum of the three sinusoids in the slow band. With an ideal filter the two signals would be exactly the same; in fact over a 2 Myr interval the largest difference was 5×10^{-5}, consistent with the expected maximum distortion in the slow band of 1×10^{-4}. Almost all of the difference arose from the sinus-

oid with a period of 2.1×10^3 yr, where the distortion is expected to be largest since the frequency lies near the edge of the slow band.

A further check is to carry out the filter/decimation process with a different initial sampling interval, which should shift the location of any aliased spectral peaks. We have performed a 10^5 yr integration with sampling interval $\Delta t' = 48$ days $= 1.33\Delta t$. The differences in the filtered orbital elements caused by the change in sampling interval were small. The largest differences appeared in Saturn's h_{eq} and k_{eq} and were $\lesssim 5\times10^{-4}$; these arise from the 5:2 near resonance between Jupiter and Saturn, whose period of $\simeq 1\times10^3$ yr is near the frequency at which filter B begins to suppress strongly the frequency response. Thus the differences arise because the near-resonant response was suppressed more strongly with the longer sampling interval. For the Earth, the largest differences in h_{eq}, k_{eq}, p_{eq}, q_{eq}, the fractional semimajor axis, or any component of the spin unit vector were $\lesssim 3\times10^{-6}$.

3.5 Accuracy of the Orbit Integration

Accuracy checks are of two kinds: physical, to ensure that our equations of motion yield trajectories that agree with more accurate but shorter integrations, and numerical, to ensure that our integration scheme accurately follows our equations of motion.

The principal physical check on the integrations is a comparison of the planetary positions with DE 102 at the earliest epoch computed in DE 102. Using a 0.25 day stepsize, we integrated back to JD 1206160.5 (roughly 1410 BC). The fractional differences $|\mathbf{r} - \mathbf{r}_{DE102}|/|\mathbf{r}|$ at this epoch were less than 3×10^{-5} for all planets. The differences are mainly in the angular coordinate and presumably reflect mostly differences in mean motion; if so, they will grow linearly with time, and after 3 Myr should not exceed 0.03 radians.

We now describe the numerical checks we have carried out.

The 3 Myr integration revealed an unexpected problem with our integration method. Figure 2 shows $\Delta a/a \equiv [a(t) - a_0]/a_0$ for each of the nine planets, where $a(t)$ is the smoothed semimajor axis and $a_0 = a(t_0)$ at the initial epoch t_0. These plots are particularly sensitive to numerical errors because the long-term variations in semimajor axis due to dynamical interactions are usually much smaller than the variations in other orbital elements. The panel for Mercury shows several jumps in $\Delta a/a$ of up to 10^{-8}, occurring at times when the integration was restarted. The size of the jumps appears to increase roughly exponentially with the interval since the last restart; after one run lasting 1.2 Myr (which was subsequently discarded) the jump was $\Delta a/a = 0.007$. This problem was discovered partway through the 3 Myr integration; in response to this discovery we decided to deliberately stop and restart future runs whenever they reached about 0.45 Myr in length. The problem was not discovered immediately because power and system failures had limited the runs in the early part of the 3 Myr integration to a maximum length of about 0.5 Myr. We have monitored the jumps in all of the orbital elements at each of the seven restarts in the 3 Myr integration: the largest jump in $|\Delta a/a|$ is 1.0×10^{-8} for Mercury and $<10^{-10}$ for any of the other planets. The largest jump in any of the other elements (h_{eq}, k_{eq}, p_{eq}, q_{eq}, and $\hat{\mathbf{a}}$) is 7×10^{-8} in Jupiter's k_{eq}. Jumps in elements other than the semimajor axis are less

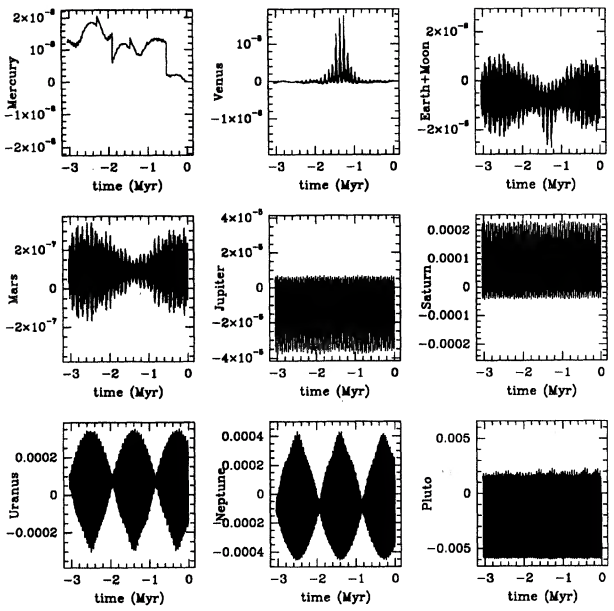

FIG. 2. The fractional change in semimajor axis $\Delta a/a \equiv [a(t) - a_0]/a_0$, where $a(t)$ is the smoothed semimajor axis and $a(t_0)$ is the value of $a(t)$ at the initial epoch t_0. The jumps in the plot for Mercury arise from numerical errors and occur when the integration is restarted (see Sec. *3.5*). The maximum and minimum smoothed semimajor axes for each planet are also given in Table 1.

serious since they do not change the mean motion. The jumps are the principal source of uncertainty in Mercury's longitude: over 3 Myr, a jump $\Delta a/a = 1\times10^{-8}$ leads to a longitude change of 1.2 radians. Fortunately, Mercury's influence on the other planets is weak, and its dominant influence is exerted through secular perturbations, which are independent of longitude.

It is difficult to explore the cause of the jumps, since they only appear after long runs. However, the following working hypothesis explains most of our findings. Consider the harmonic oscillator equation $\ddot{x} = -\omega_0^2 x$. A multistep integration scheme with stepsize h will produce numerical solutions of the form $x_n = \exp(inh\omega)$ where the principal root ω of the characteristic equation is close to ω_0. The interval of periodicity of the scheme is $(0, H_0)$ if ω is real whenever $0 < \omega_0^2 < (H_0/h)^2$ (Lambert & Watson 1976; Quinlan & Tremaine 1990). If ω_0 is large enough to lie outside the interval of periodicity, the numerical solution will contain an unstable or overstable term that leads it to diverge from the analytic solution.

It is plausible that similar behavior occurs for orbits in a Kepler potential. We hypothesize that Mercury's orbit contains weak Fourier harmonics that lie outside the interval of periodicity (Mercury has both the shortest orbital period and the highest eccentricity, so its orbit will have by far the strongest high-frequency components). These harmonics generate a slowly growing instability or overstability; in particular, an overstability would not appear in the smoothed elements (it is averaged out by the smoothing) but would lead to a jump in the orbital elements at a restart. The startup procedure for the multistep integrator would return the am-

plitude of the growing mode back to its original small value. The instability may be enhanced by mutual planetary perturbations, since a run following an isolated Mercury for > 1 Myr showed no sign of instability (Quinlan 1990).

This anomalous behavior could be reduced substantially by using a smaller stepsize than $h = 0.75$ days, but we feel that the errors that are introduced into the present integration by these effects are at an acceptable level for our purposes. A general conclusion is that the stepsize used in long solar system integrations may be determined by the need to avoid very weak numerical instabilities, rather than by the need to reproduce mean motions accurately as has usually been assumed.

As a further numerical check, we have carried out two shorter but more accurate integrations using the Störmer method: one for 0.24 Myr with step $h = 0.28125$ days, and one for 1.0 Myr with step $h = 0.375$ days (the error in the Störmer method after a fixed interval is $\propto h^{14}$ so the errors with the shorter stepsize should be reduced by a factor $(0.28125/0.375)^{14} = 0.018$). Figure 3 shows the fractional position differences $|\mathbf{r}' - \mathbf{r}|/|\mathbf{r}|$ for selected planets, where $\mathbf{r}'$ and $\mathbf{r}$ are the planetary positions in two different integrations [0.24 Myr vs 1.0 Myr in Fig. 3(a), 1.0 Myr vs 3 Myr in Figs. 3(b) and 3(c)].

The differences between the 3 and 1.0 Myr integrations in Fig. 3(b) are much larger than the differences between the 0.24 Myr and the 1.0 Myr integrations shown in Fig. 3(a); this implies that most of the differences appearing in Fig. 3(b) arise from errors in the 3 Myr integration. Mercury has by far the largest error. Figures 3(b) and 3(c), which con-

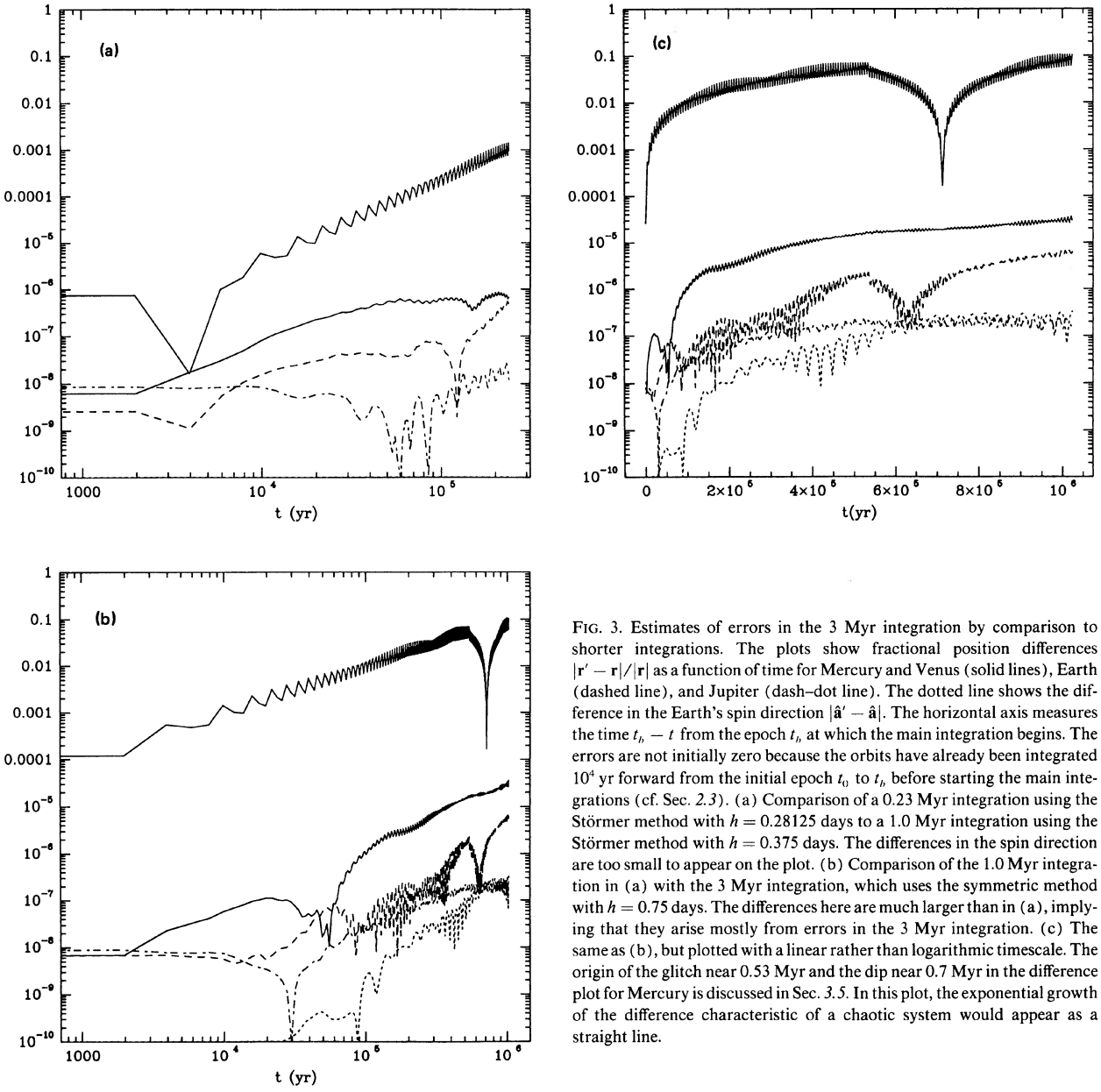

FIG. 3. Estimates of errors in the 3 Myr integration by comparison to shorter integrations. The plots show fractional position differences $|\mathbf{r}' - \mathbf{r}|/|\mathbf{r}|$ as a function of time for Mercury and Venus (solid lines), Earth (dashed line), and Jupiter (dash–dot line). The dotted line shows the difference in the Earth's spin direction $|\hat{\mathbf{a}}' - \hat{\mathbf{a}}|$. The horizontal axis measures the time $t_h - t$ from the epoch t_h at which the main integration begins. The errors are not initially zero because the orbits have already been integrated 10^4 yr forward from the initial epoch t_0 to t_h before starting the main integrations (cf. Sec. *2.3*). (a) Comparison of a 0.23 Myr integration using the Störmer method with $h = 0.28125$ days to a 1.0 Myr integration using the Störmer method with $h = 0.375$ days. The differences in the spin direction are too small to appear on the plot. (b) Comparison of the 1.0 Myr integration in (a) with the 3 Myr integration, which uses the symmetric method with $h = 0.75$ days. The differences here are much larger than in (a), implying that they arise mostly from errors in the 3 Myr integration. (c) The same as (b), but plotted with a linear rather than logarithmic timescale. The origin of the glitch near 0.53 Myr and the dip near 0.7 Myr in the difference plot for Mercury is discussed in Sec. *3.5*. In this plot, the exponential growth of the difference characteristic of a chaotic system would appear as a straight line.

tain the same data with logarithmic and linear timescales, show a small glitch in Mercury's error near 0.53 Myr. The glitch is associated with the restart of the integration at 0.527 Myr. During the restart Mercury's semimajor axis jumped by $\delta a/a = 1\times10^{-8}$, which was enough to reverse the slow growth in the longitude difference. Because of this reversal, the difference passed through a minimum near 0.7 Myr which shows up prominently in the figure.

Extrapolation of the errors in Fig. 3(b) suggests that the fractional error after 3 Myr is about 0.3 in Mercury's orbit and $\lesssim 10^{-4}$ for all the other planets.

Differences in the smoothed orbital elements between the 1.0 and 3 Myr integrations are much smaller than the differences in longitudes. Over the entire 1 Myr interval, the largest difference in $a, h_{eq}, k_{eq}, p_{eq}, q_{eq}$ for any planet, or in the Earth's spin direction $\hat{\mathbf{a}}$, is 1.1×10^{-5} (in Mars' h_{eq}). The largest difference in any of the Earth's elements is 4.7×10^{-6} in k_{eq}.

The smoothed semimajor axis of Venus exhibits an unusual burst of oscillations between 0.9 and 1.8 Myr (Fig. 1), and it is important to check that this is not due to some numerical error. We may do so using the 1.0 Myr run, which clearly shows the start of the burst (the maximum amplitude attained before the 1.0 Myr run was terminated is $\Delta a/a = 2\times10^{-9}$). For comparison, the maximum difference in $\Delta a/a$ between the 1.0 and 3 Myr runs is less than 4×10^{-12}, a factor 500 smaller. Thus the burst is almost certainly a real feature of the solution to the equations of motion.

Energy conservation is not very useful as an accuracy check, because the energy is dominated by the giant planets, while the integration errors are largest for the inner planets. An additional problem is that the equations of motion (6) do not exactly conserve the usual Newtonian energy because of the general relativistic corrections and the tidal evolution of the lunar orbit. Thus the Newtonian energy varied over a range $\Delta E/E = 3\times10^{-9}$ in the first 10^5 yr of our 3 Myr integration, but the corresponding variation in an integration with the relativistic and lunar corrections removed was only 6×10^{-11}, a factor of 50 smaller.

In summary, the tests described here suggest that the uncertainty in Mercury's longitude at the end of the 3 Myr integration is of order 1 radian, and the uncertainties in the longitudes of the other planets are far smaller.

Appendix B contains the positions and velocities of the planets and the direction of the Earth's spin axis at the end of the integration.

3.6 Accuracy of the Spin Axis Integration

We have carried out two physical checks on the accuracy of the spin axis integration.

Over short intervals (a few thousand years) the orientation of the spin axis can be compared with the power series used in practical computations of precession. For example, the obliquity of the ecliptic (the angle between the mean equator of the Earth and the mean orbital plane of the Earth) is given by (Laskar 1986)

$$\epsilon_L = 23.439291^\circ + \sum_{k=1}^{10} e_k T^k, \tag{28}$$

where T is the time in Julian centuries (1 Julian century = 36525.0 days) from J 2000.0 (JD 2451545.0) and the first three coefficients, in degrees, are $e_1 = -0.0130026$, $e_2 = -4.31\times10^{-8}$, $e_3 = 5.55347\times10^{-7}$. The resulting values for ϵ_L can be compared to $\epsilon_n = \cos^{-1}(\hat{\mathbf{a}}\cdot\hat{\mathbf{b}})$, computed from the numerical integration.

Figure 4 shows $\epsilon_L - \epsilon_n$ for the past 2000 yr. The rms difference is about 2×10^{-6} radians or 0.4 arcsec and any systematic differences are much smaller. During this period the obliquity changes by 4.5×10^{-3} radians, so the obliquity changes predicted by the power series agree with those predicted by the numerical integration with a fractional error $\ll 5\times10^{-4}$. Note that ϵ_n is not exactly the same as ϵ_L, both because $\hat{\mathbf{a}}$ differs slightly from the mean spin axis (see Sec. *2.3*) and because $\hat{\mathbf{b}}$ is the normal to the instantaneous ecliptic rather than the mean ecliptic. The two differences each contribute short-period oscillations of amplitude about 0.5 arcsec to the difference $\epsilon_L - \epsilon_n$, and these oscillations account for most of the signal shown in Fig. 4.

We can also compare the orientation of the pole $\hat{\mathbf{a}}$ to a power series solution. In the DE 102 coordinate system, the coordinates of the mean spin axis $\hat{\mathbf{a}}_m$ at time T' should be

$$\begin{aligned} a_{m,x} &= \sin\theta_A \cos(\zeta_A + \alpha_\cdot), \\ a_{m,y} &= -\sin\theta_A \sin(\zeta_A + \alpha_\cdot), \\ a_{m,z} &= \cos(\theta_A), \end{aligned} \tag{29}$$

where $\alpha_\cdot = -0.40$ arcsec enters because the DE 102 x axis differs slightly from the usual equinox. The precession parameters relative to the epoch of DE 102 (B1950.0) are given by Lieske *et al.* (1977) as

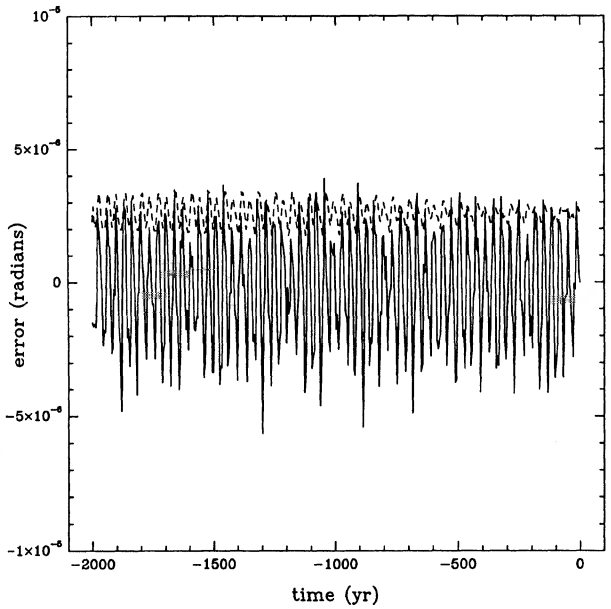

FIG. 4. The solid line shows the difference between the obliquity determined from the 3 Myr integration and the power series expansion (28) of Laskar (1986). Most of the difference arises because Laskar's expansion is based on the mean spin and the mean ecliptic, whereas the numerical results are based on the instantaneous ecliptic and the mean spin modified by nutation terms due to the Sun (see Sec. *3.6*). The dashed line shows the angle between the spin direction determined from the numerical integration and the power series expansion given by Lieske *et al.* (1977). Most of the difference arises from the nutation terms due to the Sun (see text).

$$\zeta_A = 0.6404221°T' + 0.00008390°T'^2 + 0.000005000°T'^3,$$
$$\theta_A = 0.5568715°T' - 0.00011848°T'^2 - 0.000011620°T'^3, \quad (30)$$

and $T' = t - \text{B1950.0} = t - \text{JD } 2433282.423$ measured in Julian centuries.

Figure 4 also shows the angle between the mean spin axis $\hat{\mathbf{a}}_m$ determined from Eq. (29) and the spin axis $\hat{\mathbf{a}}$ obtained from the numerical integration. During the interval shown in the figure, the spin axis orientation changed by 0.19 radians. The difference of about 0.6 arcsec arises from the dominant nutation term, which causes $\hat{\mathbf{a}}$ to precess around $\hat{\mathbf{a}}_m$ (see Sec. *2.3*). Thus, both comparisons in Fig. 4, for the obliquity and the spin axis direction, exhibit no significant deviations between the numerical integration and the usual power series.

To obtain a numerical check on the accuracy of the spin axis integration, we have monitored the angle between the spin axis directions in the 3 Myr run and in the 1 Myr run with shorter stepsize. This angle is shown by a short-dashed line in Figs. 3(b) and 3(c); the angle is too small to appear in the plot in Fig. 3(a). The maximum deviation over 1 Myr was 3.2×10^{-7} radians. Another internal check on the accuracy is provided by the magnitude of the spin vector $\hat{\mathbf{a}}$, which should remain close to unity; over the entire 3 Myr run, the maximum value of $||\hat{\mathbf{a}}| - 1|$ was 2.4×10^{-12}.

4. DISCUSSION

We shall reserve a detailed analysis of the results of the 3 Myr integration for other papers. Here we make only a few preliminary comments.

The solar system is chaotic if adjacent trajectories diverge exponentially. Our best constraint on the rate of exponential divergence is provided by the comparison in Fig. 3(b) of the 3 Myr integration using the symmetric method ($h = 0.75$ days) to the 1 Myr integration using the Störmer method ($h = 0.375$ days). The differences in planetary trajectories shown in the figure generally diverge at a rate $\propto t^k$ where k is between 1 and 2. There is no sign of exponential divergence, especially in Fig. 3(c) where exponential divergence would appear as a straight line. Thus our integrations appear to rule out chaotic behavior with e-folding times (inverse Liapunov exponents) much shorter than 1 Myr. The integration is too short to exhibit the chaos with e-folding time 5 Myr determined from the calculation of Laskar (1989).

An unsurprising but nontrivial result is that all of the planets are still present after 3 Myr; no ejections or radical changes in orbital parameters have occurred.

4.1 Long-Term Variations

The slow variations in the semimajor axes are second order in the planetary masses, in contrast to variations in the eccentricities and inclinations, which are zero order in the masses (e.g., Hagihara 1961; Milani *et al.* 1987). Thus we expect the long-term variations in the semimajor axes to be small. This expectation is confirmed by the filtered semimajor axes, at least for the terrestrial planets: the maximum fractional variations $|a_{\max} - a_{\min}|/a_{\min}$ were less than 5.1×10^{-7} for all four inner planets. The maximum variations for the outer planets were larger, as much as 0.00825 for Pluto, for at least two reasons: (i) periodic variations can more easily have frequencies within the passband, because the orbital periods are longer; (ii) there are several strong near resonances between the outer planets (e.g., the 5:2 near resonance between Jupiter and Saturn, and the 3:2 resonance between Neptune and Pluto).

Figure 2 shows the fractional variations in semimajor axis in the 3 Myr run for all of the planets. As we discussed in Sec. *3.5*, the jumps in Mercury's semimajor axis arise at restarts and reflect numerical errors, while the burst of oscillations in Venus' semimajor axis between 0.9 and 1.8 Myr reflects a real feature of the solution to the equations of motion. A similar burst of oscillations appears in the Earth's semimajor axis with opposite sign (this is just visible in Fig. 2 but shows up clearly in plots with stronger low-pass filtering). The other oscillations in the Earth's semimajor axis, as well as the oscillations in the Mars semimajor axis, are due to a three-body near resonance involving Earth, Mars, and Jupiter ($4n_3 - 8n_4 + 3n_5 \simeq 0$).

The maximum fractional variation of the Earth's semimajor axis is only 3.78×10^{-8}, which confirms the usual assumption in Milankovich theory that semimajor axis variations are too small to have a noticeable effect on the annual insolation.

Figure 5 shows plots of the smoothed $h = e\sin\varpi$ vs $k = e\cos\varpi$ for each planet in the 3 Myr integration. Figure 6 shows plots of the smoothed $p = \sin(\frac{1}{2}I)\sin(\Omega)$ vs $q = \cos(\frac{1}{2}I)\cos(\Omega)$. Here I, $\varpi = \omega + \Omega$, ω, and Ω are the inclination, longitude of perihelion, argument of perihelion, and ascending node in 1950.0 ecliptic coordinates. Table 1 shows the smoothed semimajor axis, eccentricity, and inclination (relative to the 1950.0 ecliptic) of each planet at the initial epoch JD 2433280.5 as well as the maximum and minimum values of these elements achieved in the course of the 3 Myr integration.

The evolution of the smoothed orbital elements and spin axis of the Earth can be compared to the predictions of Berger's (1978) secular perturbation theory. Figures 7 and 8 show the variations over the past 1 and 3 Myr of the variables that determine the Earth's insolation: the eccentricity, the obliquity and the longitude of perihelion relative to the moving vernal equinox ω_m (the angle between the perihelion and the ascending node, measured in a reference frame whose pole is the mean spin axis at the time of measurement). The time variation of these three variables is the astronomical input to Milankovich theory. The plots also show the difference between our results and those of Berger (1978). The plots show that Berger's secular theory reproduces the main features of the behavior of the orbital elements over the last 1–1.5 Myr but becomes quite inaccurate beyond that point. Even in the recent past, the accuracy of Berger's theory is much less than the amplitude of the smallest terms retained in it. For example, Fig. 7 shows that the typical error in the obliquity in the last 1 Myr is at least 0.001 radians, which is larger than all but 6 of the 47 terms in Berger's series.

We have checked whether the differences between our results and Berger's can be removed or reduced simply by stretching the timescale in Berger's predictions, since a change of this kind would not affect the comparison with the geologic record. We have found that the rms difference in $e\sin\omega_m$ over the past 3 Myr can be reduced by 40% by expanding Berger's timescale by 0.2%, without substantially changing the rms differences in eccentricity and obliquity; however, there is no rescaling that yields a significant improvement in the eccentricity or obliquity differences.

A new solution for the secular perturbations (Berger &

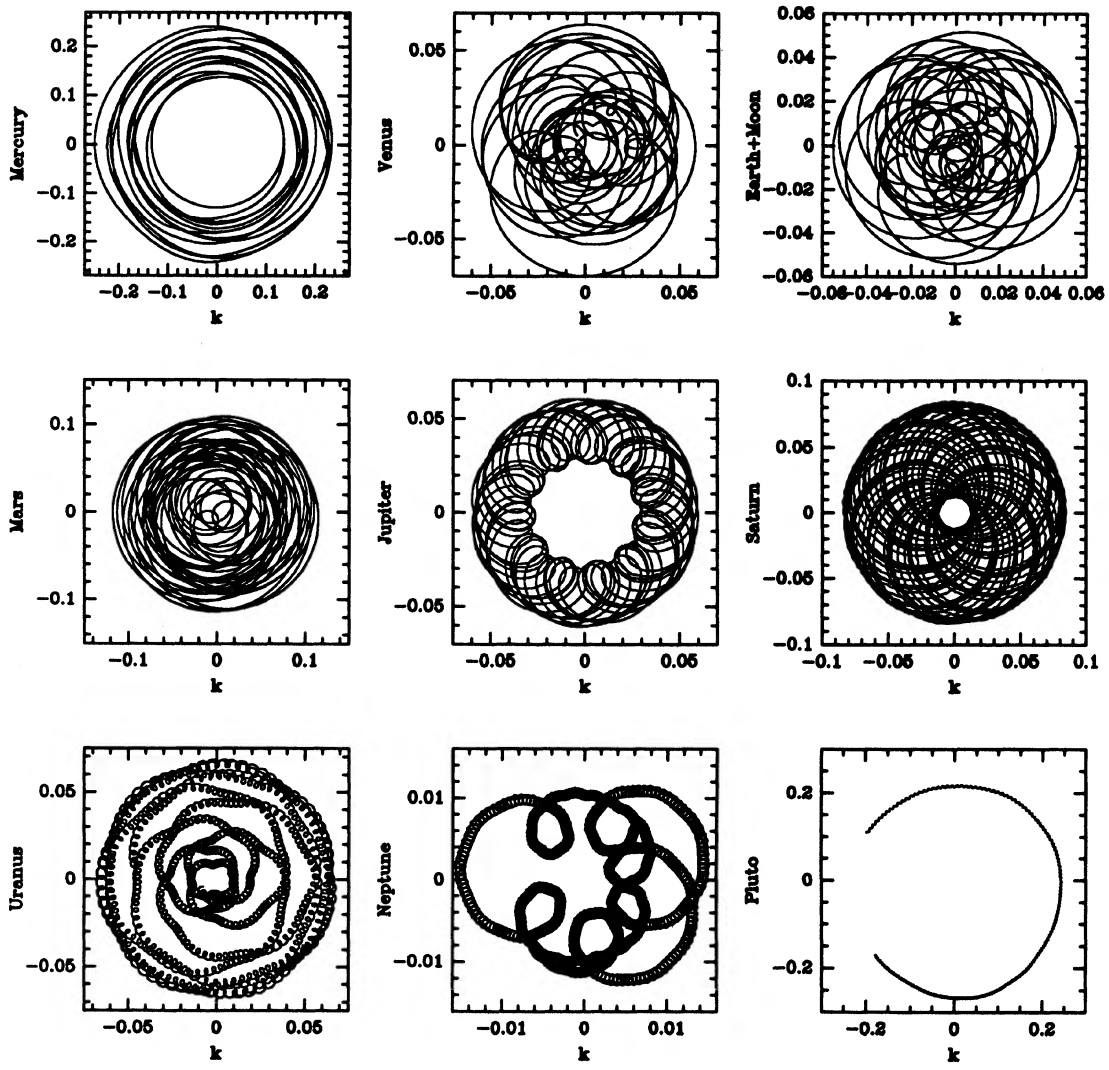

FIG. 5. Plots of the smoothed $h = e \sin \varpi$ (vertical axis) vs the smoothed $k = e \cos \varpi$ (horizontal axis) for each planet in the 3 Myr integration. The longitude of perihelion ϖ is measured in 1950.0 ecliptic coordinates.

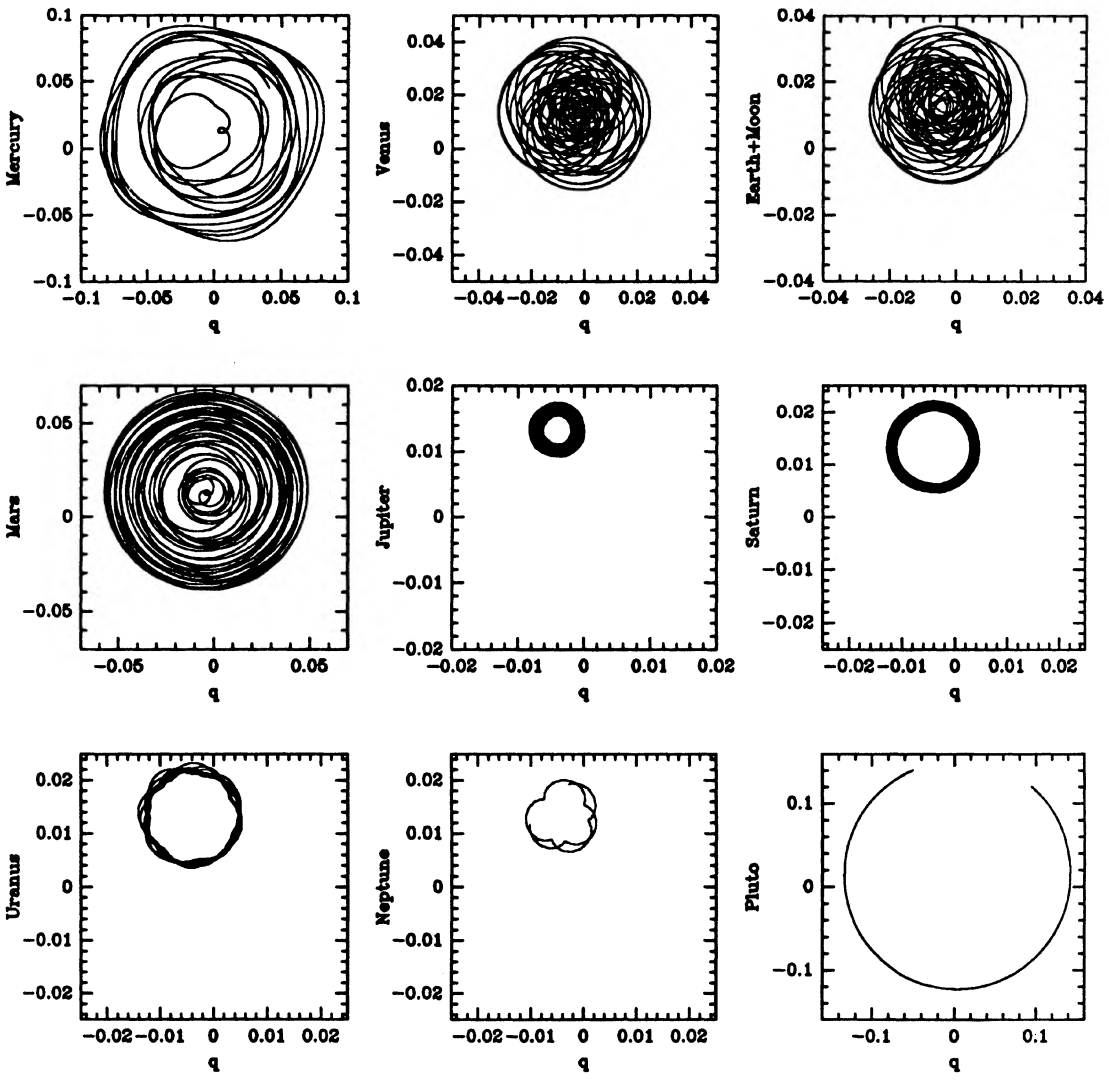

FIG. 6. Plots of the smoothed $p = \sin(\frac{1}{2}I)\sin(\Omega)$ (vertical axis) vs the smoothed $q = \sin(\frac{1}{2}I)\cos(\Omega)$ (horizontal axis) for each planet in the 3 Myr integration. Here I and Ω are the inclination and ascending node relative to 1950.0 ecliptic coordinates.

TABLE 1. Eccentricity, inclination, and semimajor axis variations.

Planet		semi-major axis (AU)	eccentricity	inclination
Mercury	now	0.38709831	0.20562	0.12224
	max	0.38709832	0.25018	0.19691
	min	0.38709831	0.12870	0.01152
Venus	now	0.7233298198	0.00680	0.05924
	max	0.7233298326	0.06992	0.08455
	min	0.7233298193	0.00029	0.00015
Earth+Moon	now	1.0000010240	0.01673	0.00000
	max	1.0000010348	0.05788	0.07482
	min	1.0000009970	0.00016	0.00000
Mars	now	1.523679205	0.09336	0.03229
	max	1.523679729	0.11767	0.13756
	min	1.523678950	0.00232	0.00160
Jupiter	now	5.202660892	0.04843	0.02279
	max	5.202696335	0.06104	0.03618
	min	5.202464518	0.02612	0.01955
Saturn	now	9.55425887	0.05537	0.04347
	max	9.55647731	0.08501	0.04539
	min	9.55384531	0.01163	0.01037
Uranus	now	19.217059	0.04718	0.01349
	max	19.223802	0.06962	0.04743
	min	19.211254	0.00632	0.00863
Neptune	now	30.113148	0.00856	0.03097
	max	30.126211	0.01584	0.04098
	min	30.099391	0.00260	0.01389
Pluto	now	39.53829	0.24897	0.29920
	max	39.63026	0.27236	0.30680
	min	39.30261	0.21379	0.24476

NOTES: Inclination is measured in radians relative to the ecliptic plane of 1950.0. "now" refers to the values of the elements at the start of the integration (J1950.0 minus 2 days), while "max" and "min" denote the maximum and minimum values attained during the 3 Myr integration. All elements have been smoothed with a low-pass filter as described in §3.4.

Loutre 1988; Berger 1990, personal communication) yields substantially better agreement with our numerical integrations.

4.2 What We Did Wrong

A somewhat smaller stepsize, say $h = 0.5$ instead of 0.75 days, should improve substantially the accuracy of the integration of Mercury's orbit, and hopefully would greatly reduce the weak numerical instability that we described in Sec. *3.5*.

The 3 Myr integration had to be restarted seven times. Each restart introduces errors, both because the startup procedure is not exact and because 10^4 yr of integration must be repeated in order to refill the filter arrays (although in this case restarts also had the beneficial effect of suppressing a weak instability in Mercury's orbit). Once the stepsize is reduced enough to suppress the instability, it would be straightforward and useful to save the arrays of past positions and accelerations at regular checkpoints (say, every few thousand years), so that the computation could be restarted cleanly.

The code was not thoroughly optimized before being run. Subsequent profiling showed that several improvements could be made. The arrays of past positions and accelerations used in the symmetric integrator are quite large (a single integration step for nine planets and the Earth's spin with a twelfth-order symmetric method using roundoff corrections involves over 2000 array elements), and manipulating these arrays used about 20% of the machine cycles; it should be possible to reduce substantially the time spent on this task, for example by using pointers. Also, about 13% of the machine cycles were spent on evaluating the velocities at every step; since these are needed only for evaluating the small relativistic corrections and the orientation of the ecliptic, there should be a faster way to do this to adequate accuracy. In our code only 25% of the cycles were spent on force evaluations and 75% were spent on advancing the positions and velocities; with more efficient programming it should be possible to reduce the time spent on the second task by a factor of 2 or more, so one might hope to speed up the code by 30% or so.

One issue that deserves further investigation is how best to start a multistep integration. The multistep methods need positions and accelerations at up to 13 steps in order to start. Our startup procedure, following Cohen *et al.* (1973), is to start with a crude approximation to the positions and accelerations and then to integrate repeatedly forward 12 steps and backward 12 steps from the initial epoch until convergence. One flaw with this procedure is that there is no simple characterization of the properties of the converged solution, nor is it necessarily unique. An alternative approach is to carry out a very accurate integration for 13 steps using a self-starting method such as Bulirsch–Stoer or Runge–Kutta before switching to the multistep method, but this has potential problems as well. The behavior of the solution of the exact differential equations is slightly different from the behavior of the solution of the difference equations, and the sudden shift from one method to the other may introduce spurious components into the solution. It is not clear what the best method is, or even what "best" means: should we aim for solutions with the smallest energy and angular momentum oscillations, or the most accurate mean motions, or the minimum amplitude of any weak numerical instabilities, or is some other criterion more useful?

Both the Störmer and symmetric methods are designed to ensure that the truncation error at each step in the integration of $\ddot{x} = -\omega^2 x$ is $O(\omega h)^k$ where the exponent k is as large as possible. This design philosophy implies that the truncation errors for the outer planets, with small ω's, will be far smaller than the errors for the inner planets. A better philosophy—analogous to the approximation of functions by Chebyshev polynomials rather than power series—might be to ensure that the maximum truncation error over the whole interval $0 < \omega h < \omega_{\max} h$ is as small as possible, where $\omega_{\max}$ is chosen in advance as the largest frequency of interest (say, several times the mean motion of Mercury).

5. SUMMARY

We have followed the orbits of the nine planets and the Earth's spin axis backwards in time for 3 Myr. We believe that the physical model, the initial conditions, and the integration procedure are accurate enough that the fractional error in the Earth's position is less than about 0.03 radians at the end of the integration. Errors in the other planets are larger, and may be as large as several radians for Mercury (due to numerical errors) and Pluto (due to inaccurate initial conditions). We have stored the phase space coordinates of all the planets and the direction of the spin axis at intervals of about 2000 yr. The orbital elements have been filtered to remove all frequencies lower than about 10^3 yr and stored at intervals of 500 yr.

The output data files, the orbital elements that determine the Earth's insolation shown in Figs. 7 and 8, and the source

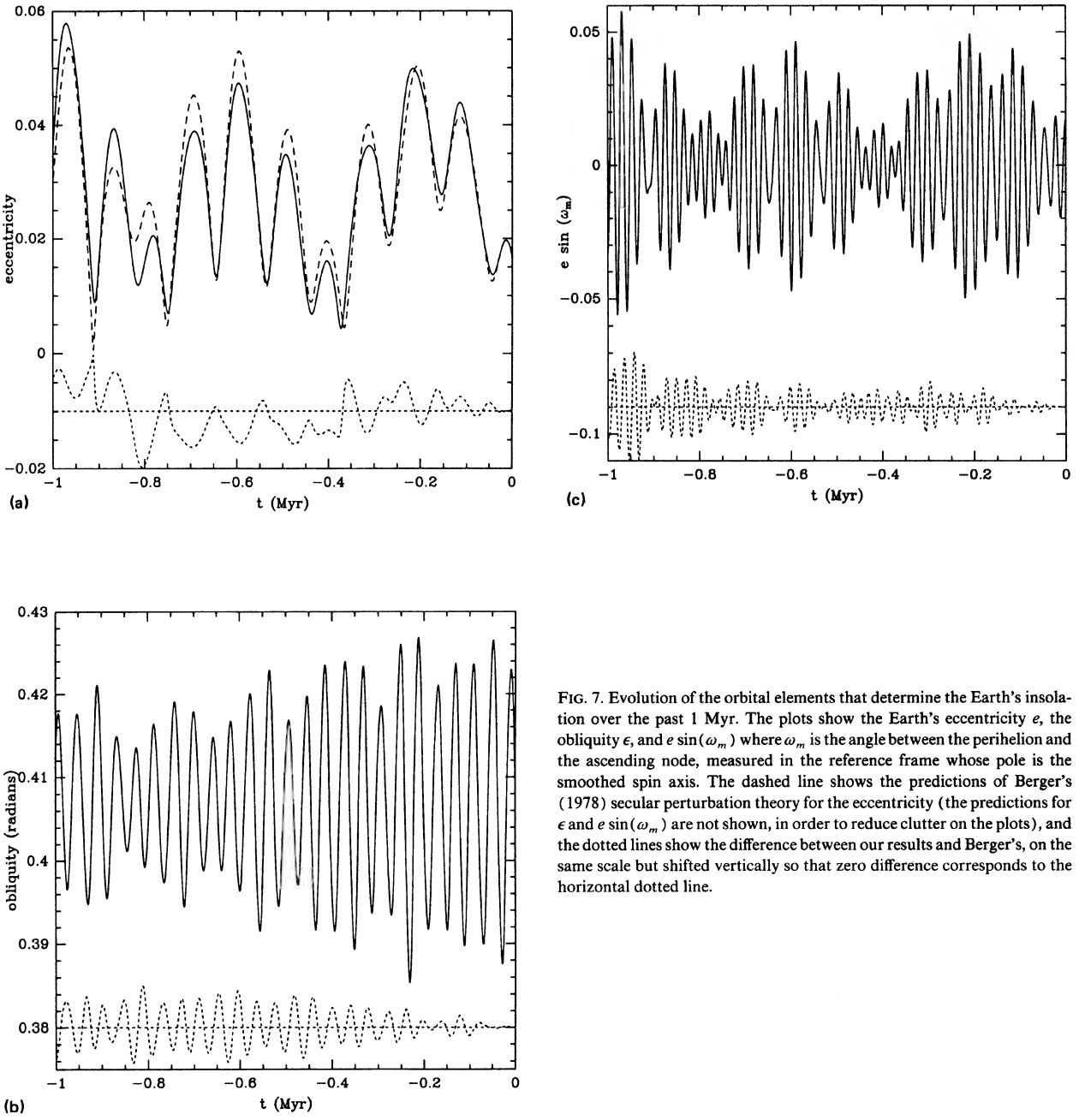

FIG. 7. Evolution of the orbital elements that determine the Earth's insolation over the past 1 Myr. The plots show the Earth's eccentricity e, the obliquity ϵ, and $e \sin(\omega_m)$ where ω_m is the angle between the perihelion and the ascending node, measured in the reference frame whose pole is the smoothed spin axis. The dashed line shows the predictions of Berger's (1978) secular perturbation theory for the eccentricity (the predictions for ϵ and $e \sin(\omega_m)$ are not shown, in order to reduce clutter on the plots), and the dotted lines show the difference between our results and Berger's, on the same scale but shifted vertically so that zero difference corresponds to the horizontal dotted line.

code are all available on request through electronic mail.

All of the planetary orbits appear to be regular on Myr timescales, since adjacent trajectories do not diverge exponentially (Fig. 3). The smoothed semimajor axes of Venus and the Earth show a burst of oscillations of maximum size $\Delta a/a \simeq 2 \times 10^{-8}$ between 1 and 2 Myr in the past; it would be interesting to determine the dynamical explanation for this oscillation.

Comparison of the smoothed orbital elements for the Earth with the predictions of secular perturbation theory (Berger 1978) shows that the secular theory predictions are inaccurate beyond about 1–1.5 Myr into the past, although a newer secular solution (Berger & Loutre 1988; Berger 1990, personal communication) agrees more closely with our numerical results.

A reflection of recent changes in computing technology is that the present integrations were carried out on a commercially available personal workstation, rather than on a supercomputer or a special-purpose machine. The slow speed of the workstation relative to a supercomputer is compensated by the large amounts of time available (the 3 Myr integration used two months of background time). Also, many supercomputers are not suitable for this task because their floating point arithmetic is not sufficiently accurate. By im-

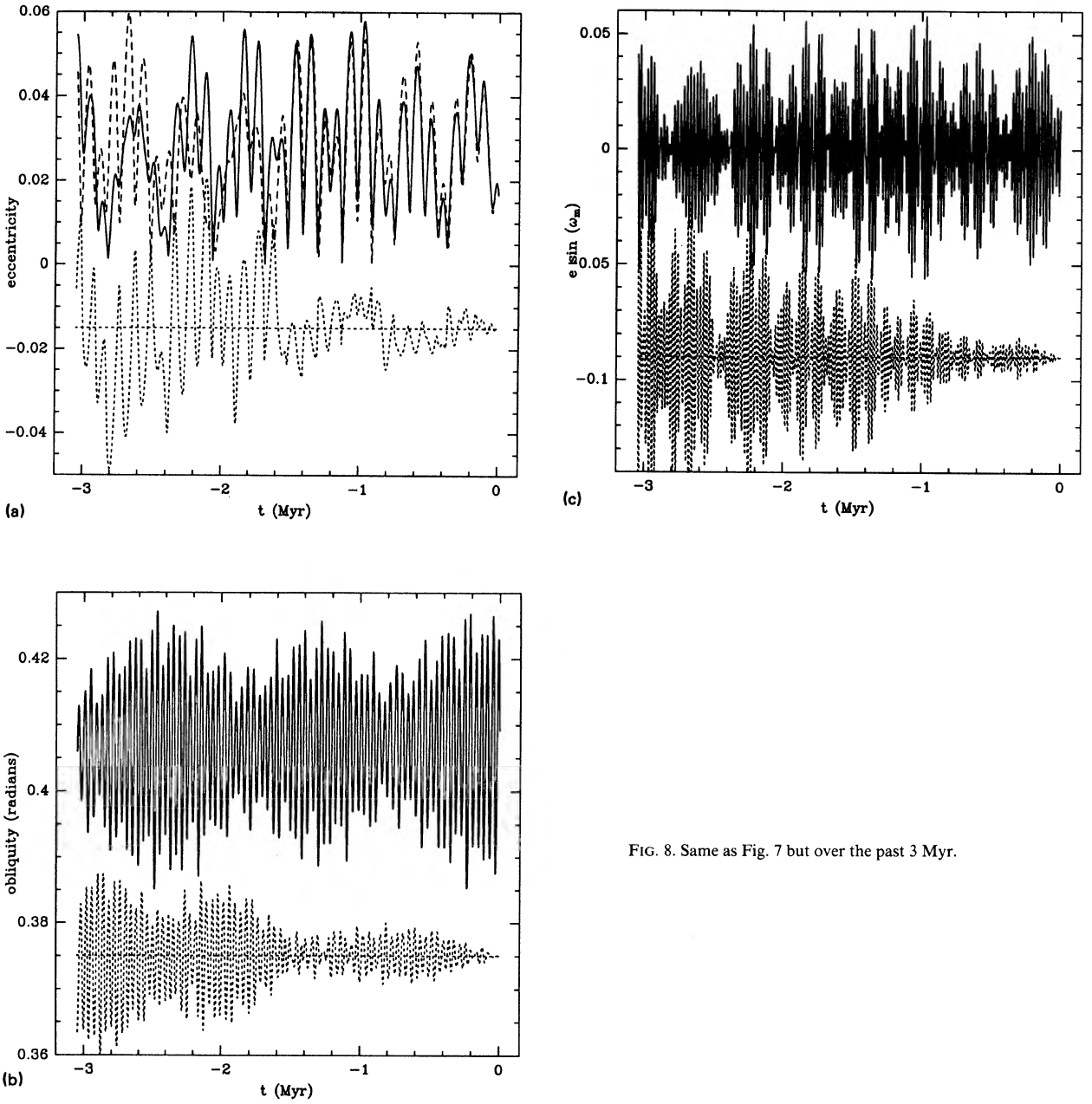

FIG. 8. Same as Fig. 7 but over the past 3 Myr.

proving our code, and by using faster small machines that should appear over the next few years, it should be possible to extend the integration span by a factor of 10 or more. A desirable long-term goal would be to carry out a 100 Myr integration, which should be long enough to determine whether the solar system is chaotic with an e-folding time of 5 Myr, as indicated by Laskar's (1989) secular perturbation theory.

Note added in proof. We have repeated the 3 Myr integration described in this paper with a smaller step size, $h = 0.5$ days instead of $h = 0.75$ days. Preliminary analysis of the results confirms several of the error estimates in Sec. *3.5*. The maximum fractional position difference $|\mathbf{r}' - \mathbf{r}|/|\mathbf{r}|$ over the 3 Myr integration interval was 1.28 for Mercury (corresponding to a longitude error of 1.35 radians); for the other planets the maximum error was $< 4 \times 10^{-4}$. The maximum difference in the filtered elements for any planet, or in the Earth's spin direction, was 6.7×10^{-5} (in Mercury's h_{eq}). The smaller step size greatly reduced the jumps in Mercury's semimajor axis occurring at restarts and allowed longer runs to be made between restarts: the largest jump in $|\Delta a/a|$ was 8×10^{-10}, more than a factor of 10 smaller than with a 0.75 day step, even though the interval between restarts was as large as 1.6 Myr.

We thank Myles Standish for providing the DE 102 ephemeris on tape, Godelieve Deblonde for providing a program

to evaluate Berger's predictions for the Earth's orbital elements, Dick Peltier for motivating us to investigate this problem and for his enthusiastic support, Gerry Quinlan for many discussions and for implementing the symmetric integration method in our code, and Josh Barnes, Dick Bond, and Arnold Boothroyd for allowing us to run many long background jobs on their workstations. This research was supported by operating grants from NSERC and by a Special Research Grant from the Connaught Fund at the University of Toronto.

APPENDIX A

We describe here the derivation of the parameters of the lunar orbit used in Eq. (2) and in setting the initial conditions for the Earth–Moon barycenter.

The parameter R that describes the radius of the lunar orbit is derived from Hill's lunar theory (e.g., Brouwer & Clemence 1961), which is based on the approximations that (i) the eccentricity of the Earth's orbit is negligible; (ii) the inclination of the lunar orbit to the ecliptic is negligible; (iii) the ratio of the solar mass to the Earth mass and the solar distance to the lunar distance are both large, in the sense that $\mathcal{M}_\odot/\mathcal{M}_\oplus \to \infty$ and 1 A.U./$R \to \infty$ while the ratio $(\mathcal{M}_\oplus/\mathcal{M}_\odot)(1\ \text{A.U.}/R)^3$ remains fixed. Hill's analysis is based on an orbit called the variation orbit, which (i) lies in the ecliptic; (ii) is periodic in a frame rotating with the Earth's orbit; (iii) has the same mean angular speed as the lunar orbit. In Cartesian coordinates, the variation orbit can be expanded as a Fourier series,

$$(x,y) = \sum_{j=0}^{\infty} (a_j \cos(2j+1)\tau, b_j \sin(2j+1)\tau), \qquad \text{(A1)}$$

where $\tau = (n_L - n_\odot)(t - t_0)$, $n_L = 2\pi/(27.32166\ \text{days})$ is the mean angular speed of the Moon in an inertial frame, $n_\odot = 2\pi/(365.2564\ \text{days})$ is the angular speed of the Sun, the (x,y) plane is the ecliptic plane, the origin is the Earth, and the x axis points towards the Sun. If we consider only the largest terms, $j = 0$, the orbit is an ellipse with semi-axes a_0 and b_0, and we arbitrarily take $R = \frac{1}{2}(a_0 + b_0)$ (R is called the "scale factor for the variation orbit" by Brouwer & Clemence 1961). Hill's theory yields $R/a = 0.99909$, where a is defined by $G(\mathcal{M}_\oplus + \mathcal{M}_L) = n_L^2 a^3$; we find $a = 0.0025719$ A.U. $= 3.8475 \times 10^{10}$ cm and $R = 0.0025695$ A.U. $= 3.8440 \times 10^{10}$ cm using the DE 102 mass ratios $\mathcal{M}_\odot/(\mathcal{M}_\oplus + \mathcal{M}_L) = 328900.53$ and $\mathcal{M}_\oplus/\mathcal{M}_L = 81.3007$.

The first contribution to the correction factor f in Eq. (2) arises because the variation orbit is not exactly circular. If the Moon followed the variation orbit exactly, the force per unit mass on the Earth–Moon system due to the Sun would be [compare Eq. (2)]

$$-\frac{G\mathcal{M}_\odot}{r^3}\mathbf{r} - \frac{3G\mathcal{M}_\odot \mathcal{M}_\oplus \mathcal{M}_L}{4(\mathcal{M}_\oplus + \mathcal{M}_L)^2}\frac{4\langle x^2\rangle - 2\langle y^2\rangle}{r^5}\mathbf{r}, \qquad \text{(A2)}$$

where $\langle\cdot\rangle$ denotes a time average. Taking coefficients for the Fourier series (A1) from the table on p. 348 of Brouwer & Clemence (1961), we have $4\langle x^2\rangle - 2\langle y^2\rangle = \Sigma_{j=0}^{\infty}(2a_j^2 - b_j^2) = 0.94790R^2$. Thus the deviation of the variation orbit from circular yields a correction factor $f_H = 0.9479$.

A second correction arises because of the inclination i_L between the lunar orbit and the ecliptic, which yields a correction factor $f_i \equiv (1 - \frac{3}{2}\sin^2 i_L) = 0.9879$. Additional, smaller corrections arise from several sources. The free eccentricity e_L of the lunar orbit, which corresponds to a deviation from the variation orbit, increases the acceleration by a factor $f_e \equiv (1 + \frac{3}{2}e_L^2) = 1.0045$. Another correction (known as the evection) arises from variations in the lunar eccentricity e_L and argument of pericenter ϖ_L with argument $2(\lambda_\odot - \varpi_L)$, where $\lambda_\odot$ is the solar longitude. The evection contributes a correction factor $f_{\text{ev}} = 1 + \frac{225}{8}(n_\odot/n_L)e_L^2 = 1.0063$. Finally, the principal perturbation in the latitude (the inclination and precession rate of the lunar orbit depend on the angle between the lunar node and the Earth–Sun line) yields a correction $f_{\text{lat}} = 1 + \frac{9}{8}(n_\odot/n_L)\sin^2 i_L = 1.0007$. Overall, the correction is

$$f = f_H f_i f_e f_{\text{ev}} f_{\text{lat}} = 0.9473. \qquad \text{(A3)}$$

A limited check on this result is provided by comparison of two integrations with $f = 0$ and $f = 0.9473$ to the DE 102 ephemeris. The integration with $f = 0$ exhibited angular differences from DE 102 that were larger for the Earth–Moon barycenter than for any other planet, by a factor exceeding 100. With $f = 0.9473$ the angular differences for the Earth–Moon system were comparable to those for the other planets, suggesting that our value of the correction factor is accurate to within about 1%.

Our approximate treatment of the Moon also affects the initial conditions. The principal periodic component in the disturbing function acting on the Earth–Moon barycenter is

$$\mathcal{R} = \frac{3G\mathcal{M}_\odot \mathcal{M}_\oplus \mathcal{M}_L}{4(\mathcal{M}_\oplus + \mathcal{M}_L)^2}\frac{R^2}{a^3}\cos 2(\lambda_\odot - \lambda_L), \qquad \text{(A4)}$$

where λ_L and $\lambda_\odot$ are the mean longitudes of the Moon and Sun as viewed from Earth. As viewed from the Sun, the Earth's mean longitude is $\lambda = \lambda_\odot + \pi$, and Lagrange's equation $da/dt = 2/(na)(\partial\mathcal{R}/\partial\lambda)$ yields

$$a = a_0 - \frac{3}{2}\frac{n_\odot}{n_L - n_\odot}\frac{R^2}{a}\frac{\mathcal{M}_\oplus \mathcal{M}_L}{(\mathcal{M}_\oplus + \mathcal{M}_L)^2} \times \cos 2(\lambda_\odot - \lambda_L) \equiv a_0(1 - \delta). \qquad \text{(A5)}$$

The periodic term is not present in our integrations since the Moon is replaced by a ring. Thus it should be removed from the initial conditions, that is, the DE 102 initial semimajor axis a should be replaced by a_0, by rescaling the initial position and velocity vectors by factors $(1 + \delta)$ and $(1 - \frac{1}{2}\delta)$, respectively. At the initial epoch, JD 2433280.5, $\cos 2(\lambda_\odot - \lambda_L) = -0.503$ and $\delta = -4.83 \times 10^{-9}$.

APPENDIX B

In this Appendix we list the masses and initial and final phase-space coordinates of all the planets and the direction of the Earth's spin axis. The coordinates are printed with 15 significant figures; this precision is provided to help test reproducibility and does not represent the accuracy of either the initial conditions or the integration itself. The first line after each planet contains the positions in A.U. (A.U. $= 1.49597870 \times 10^{13}$ cm) and the second line contains the velocities in A.U./day. In these units $G\mathcal{M}_\odot = k^2$ where $k = 0.01720209895$. The coordinates are in the DE 102 reference frame.

The initial conditions are taken from DE 102, except that the position and velocity of the Earth–Moon barycenter have been adjusted slightly to remove the principal oscillation with a period of one synodic month (see Appendix A).

Body	Inverse mass
Mercury	6023600
Venus	408523.5
Earth + Moon	328900.53
Mars	3098710
Jupiter	1047.355
Saturn	3498.5
Uranus	22869
Neptune	19314
Pluto	3000000

Initial epoch: JD 2433280.5

```
Positions (first line) and velocities (second line) in AU
and AU/day:
Mercury:
0.343926450169642 0.0456154799533135 -0.0109240372119325
-0.00846653204500986 0.0256146053072818 0.0145868453362396
Venus:
.142965184343246 .647005066033887 .28248240066038
-0.0198938122793425 0.00311311946611859 0.0026594458057458
Earth+Moon barycenter:
-.136364695954795 .893397922857 .387458344639337
-0.0173199988485296 -0.00224430473176756 -0.000973361115758044
Mars:
-1.36983397618342 .843135248017904 .42383290661143
-0.00738456383127117 -0.0094773586392742 -0.00415165513666213
Jupiter:
3.34936422369601 -3.47376144901258 -1.5721496863938
0.00558564314958231 0.00496226113722251 0.00199227692673937
Saturn:
-8.97250506828211 2.27968200813286 1.33033860971146
-0.00185825195699671 -0.00498385858141744 -0.00198025741280725
Uranus:
-1.00300399532732 17.3235084732718 7.60482504641591
-0.00395525416301772 -0.000375913785112941 -0.000108849991287794
Neptune:
-29.1945807386112 -7.71928519199847 -2.42724537828877
0.000820748057818085 -0.00277209825958023 -0.00115611603043592
Pluto:
-26.2336507820155 20.5619754200559 14.4445571277807
-0.00131588869828116 -0.00262012820549352 -0.000427083355026298

components of unit vector along the Earth's spin axis:
1.51920829e-07 -2.57060482e-06 .999999999996684
```

Final epoch: JD −1113787075.5

```
Mercury:
-0.352947405541961 -0.286054504716246 -0.0569819590510637
0.016295248990639 -0.0143206218982002 -0.00758313563615676
Venus:
-0.380913939194714 0.565289687859575 0.257082796674093
-0.0174494014611548 -0.00936394516118103 -0.00333216019926604
Earth+Moon barycenter:
-1.05201474735186 -0.0542535463736323 0.0134552313064028
0.000614064145209407 -0.0148654135096302 -0.00667104240247104
Mars:
0.866886281616371 -1.06166694962047 -0.317054267231078
0.0120790553204725 0.00821890368124034 0.0036066212623375
Jupiter:
2.9949220214064 3.64053149916691 1.48312294702764
-0.00621590764541165 0.00446562612798769 0.00208654440117861
Saturn:
-9.78277568052112 0.960212059646976 0.67524632267954
-0.000428326030567897 -0.00498576594765095 -0.00200328891035628
Uranus:
-18.2088483587854 -5.29200056804054 -1.90833525162376
0.00115534925556441 -0.00344121330796791 -0.00156234924128551
Neptune:
-23.7237940834069 -16.870153528335 -6.20262562269402
0.00190716703546912 -0.00229379568223938 -0.00105774715760987
Pluto:
45.2828079995853 3.29157399772757 -11.3188599363404
-8.61125353708303e-05 0.00185794398606613 0.00129225834956751

components of unit vector along the Earth's spin axis:
-0.0788170256279992 -0.0361574629946856 0.996233162638049
```

REFERENCES

ANSI/IEEE 1985, IEEE Standard for Binary Floating-Point Arithmetic, Std 754-1985 (IEEE, New York)

Applegate, J. H., Douglas, M. R., Gürsel, Y., Sussman, G. J., and Wisdom, J. 1986, AJ, 92, 176

Berger, A. L. 1978, J. Atmospheric Sci., 35, 2362

Berger, A. 1980, Vistas Astron., 24, 103

Berger, A. 1990, personal communication

Berger, A., and Loutre, M. F. 1988, Scientific Report 1988/13, Institut d'Astronomie et de Geophysique G. Lemaitre, Université Catholique de Louvain

Brouwer, D., and Clemence, G. 1961, Methods of Celestial Mechanics (Academic, New York)

Carpino, M., Milani, A., and Nobili, A. M. 1987, A&A, 181, 182

Cohen, C. J., Hubbard, E. C., and Oesterwinter, C. 1973, Astron. Papers Amer. Ephemeris, 22, 1

Dekker, T. J. 1971, Numer. Math., 18, 224

Dickey, J. O., and Williams, J. G. 1982, EOS, 63, 301

Gear, C. W. 1971, Numerical Initial Value Problems in Ordinary Differential Equations (Prentice-Hall, Englewood Cliffs)

Goldreich, P. 1966, Rev. Geophys., 4, 411

Hagihara, Y. 1961, in Planets and Satellites, edited by G. P. Kuiper and B. M. Middlehurst (University of Chicago Press, Chicago), p. 95

Hamming, R. W. 1983, Digital Filters, 2nd ed. (Prentice-Hall, Englewood Cliffs)

Imbrie, J. 1982, Icarus, 50, 408

Kinoshita, H. 1975, Smithsonian Astrophysical Observatory Special Report, 364

Kinoshita, H. 1977, Celest. Mech., 15, 277

Kinoshita, H., and Nakai, H. 1984, Celest. Mech., 34, 203

Kubo, Y., and Fukushima, T. 1988, in The Earth's Rotation and Reference Frames for Geodesy and Geodynamics, edited by A. K. Babcock and G. A. Wilkins (Reidel, Dordrecht), p. 331

Knuth, D. E. 1981, The Art of Computer Programming, 2nd ed. (Addison-Wesley, Reading), Vol. 2

Lambeck, K. 1980, The Earth's Variable Rotation: Geophysical Causes and Consequences (Cambridge University Press, Cambridge)

Lambert, J. D., and Watson, I. A. 1976, J. Inst. Maths. Applics., 18, 189

Laskar, J. 1986, A&A, 157, 59

Laskar, J. 1989, Nat, 338, 237
Lieske, J. H., Lederle, T., Fricke, W., and Morando, B. 1977, A&A, 58, 1
Milani, A., Nobili, A. M., and Carpino, M. 1987, A&A, 172, 265
Newhall, X X, Standish, E. M., and Williams, J. G. 1983, A&A, 125, 150
Press, W. H., Flannery, B. P., Teukolsky, S. A., and Vetterling, W. T. 1986, Numerical Recipes (Cambridge University Press, Cambridge)
Quinlan, G. D. 1990, private communication
Quinlan, G. D., and Tremaine, S. 1990, AJ, 100, 1694
Quinn, T., and Tremaine, S. 1990, AJ, 99, 1016
Richardson, D. L., and Walker, C. F. 1987, in Astrodynamics 1987 (Advances in the Astronautical Sciences, Vol. 65), edited by J. K. Soldner, A. K. Misra, R. E. Lindberg, and W. Williamson (Univelt, San Diego), p. 1473
Richardson, D. L., and Walker, C. F. 1989, J. Astronautical Sci., 37, 159
Roy, A. E., Walker, I. W., Macdonald, A. J., Williams, I. P., Fox, K., Murray, C. D., Milani, A., Nobili, A. M., Message, P. J., Sinclair, A. T., and Carpino, M. 1988, Vistas Astron., 32, 95
Standish, E. M. 1990, A&A, 233, 252
Standish, E. M., and Hellings, R. W. 1989, Icarus, 80, 326
Sussman, G. J., and Wisdom, J. 1988, Sci, 241, 433
Weinberg, S. 1972, Gravitation and Cosmology (Wiley, New York)
Will, C. M. 1981, Theory and Experiment in Gravitational Physics (Cambridge University Press, Cambridge)